Development of an Ultra Stable Fiber Optic Frequency Distribution System Using an Optical Delay Control Module

Katsuhisa Sato

Doctor of Engineering

Department of Astronomical Science
School of Mathematical and Physical Science
The Graduate University for Advanced Studies

2000

Development of an Ultra Stable

Fiber Optic Frequency Distribution System

Using an Optical Delay Control Module

Katsuhisa Sato

TABLE OF CONTENTS

ABSTRACT

An ultra stable fiber optic frequency distribution system is described. One of the purposes in developing the ultra stable frequency distribution system is to apply the system for distribution of a reference frequency supplied by an atomic frequency standard. The frequency stability level of a hydrogen maser frequency standard which is widely used, is around (2 to 3)$\times 10^{-15}$ for the integration time of 1000 second in Allan standard deviation (ASD). On the other hand, a long term stability of a linear ion trap frequency standard is less than 1×10^{-16} /day, a factor of 30 time improvement over hydrogen masers. Therefore, an ultra stable frequency distribution system with phase stability level of 1×10^{-16} in ASD for 1000 second averaging time is required. A phase-stable frequency distribution system is also a key instrument for the very long baseline interferometer (VLBI) as well as regular connected radio interferometer. Specifically, the stability level in ASD of 10^{-16} for the averaging time of 1000 second is required in the frequency distribution system for the differential VLBI in precise measurements of the distance to galactic radio sources and the connected radio interferometer in sub-millimeter range.

The ultra stable phase stability of the developed fiber optic frequency distribution system is achieved by configuring a closed phase-locked loop with an optical fiber transmission line in which two optical carrier signals with different wavelengths are transmitted as a forward and a backward signal, and installing an

optical delay control module which has no differential dispersion effect between the two optical carrier waves and induces no electrical noise. This is the first ODM application to be implemented for use in fiber optic frequency distribution system. A phase stabilized optical fiber (PSOF) is used for the signal transmission line.

The frequency stability measurement system, of which resolution is the order of 10^{-17} for 1000 second integration time, has been designed to measure the stability of developed fiber optic frequency distribution system. A vector voltmeter is applied to make the frequency stability measurement system as state-of-the-art specification. The vector voltmeter outputs a DC analog signal proportional to compared phase difference between reference signal and test signal as direct analog output. This is the first direct DC analog output usage of a vector voltmeter to be implemented for use in a frequency stability measurement system. The system noise level of this measurement system in the laboratory is better than any dual mixer time difference systems.

The stabilities of the developed ultra stable fiber optic frequency distribution system in ASD are 7.5×10^{-17} and 1.1×10^{-17} at 1000 second and 10,000 second averaging time respectively while the environmental temperature of the PSOF cable varies in the range of 10°C and at the rate of 10°C/12hours. This system has the best stability in frequency distribution systems so for and enough stability to apply for the linear ion trap frequency standard or the differential VLBI.

CHAPTER 1

INTRODUCTION

1.1 Objectives of the Thesis

Ultra stable frequency standards have been researched and developed to achieve better frequency stability in many institutes. The frequency stability level of a hydrogen maser frequency standard is around (2 to 3)$\times 10^{-15}$ for the integration time of 1000 second in Allan standard deviation (ASD). A liner ion trap frequency standard has been researched and developed lately [9]. The developed mercury linear ion trap frequency standard could achieve a short term stability performance of $\sigma_y(\tau) = 2\times 10^{-14} / \tau^{1/2}$ when it was operated with an appropriate local oscillator. On the other hand, the long-term stability design goal was to achieve an average frequency drift rate of less than 1×10^{-16} /day, a factor of 30 time improvement over hydrogen masers. These frequency standards are still under development and more stable frequency standards would be announced. An ultra stable frequency distribution system that surpasses the phase stability level of 10^{-16} in ASD for 1000 second averaging time is required to distribute a stable frequency source without degrading its stability.

In the differential very long baseline interferometer (VLBI) observations, the

delay path length for a target source is measured relative to that for a reference source to reduce the variations of the path length caused by the atmospheric fluctuation [10]. The phase errors are caused not only by atmospheric fluctuations, but also from various parts of the observation instruments such as gravitational deformation of an antenna, a front-end receiver, a local oscillator for a frequency down conversion, a signal transmission line for IF signal, a reference signal transmission line for a local oscillator, a delay calibration unit and an analog-to-digital (A/D) converter in a VLBI sampler unit. The total phase error is given by the root-sum-squares (RSS) of the phase variations caused in the individual parts of the instruments and the atmosphere. Assuming all of these phase errors is equal, the allowed value of the phase error in the frequency distribution system is assigned as one third of the total phase errors. Thus, a phase-stable frequency distribution system is also a key instrument for the VLBI as well as regular connected radio interferometer. Specifically, the stability level in ASD of 10^{-16} for the averaging time of 1000 second is required in the frequency distribution system for the differential VLBI in precise measurements of the distance to galactic radio sources [10] and the connected radio interferometer in sub-millimeter range.

Lutes installed a 3km experimental multi mode optical fiber link operating at an 850nm wavelength at Jet Propulsion Laboratory (JPL) in 1979. This system was to be used in the development of ultra-stable frequency and timing distribution systems. The link achieved a stability of 4×10^{-15} for 100 second integration time at 100MHz. Lutes et al. developed a single-mode fiber capability at JPL in 1986. After the experiment was completed, the link was set up for one-way distribution of the signal between two stations and was used as the station reference for a successful connected element interferometry experiment. The stability of this link was better than 1.5×10^{-15} for 1000 second integration time at 100MHz because of the improved

signal-to-noise ratio (SNR) and stability of the link over the one way path length [2]. Lutes applied an optical isolator to the 850m length fiber-optic frequency reference distribution link achieving the stability about 2.5×10^{-15} for 1000 second integration time at 100MHz in 1989 [13]. Primas et al. tested an active stabilization of a fiber-optic frequency distribution system at JPL in 1989. The method for actively controlling the phase variations in the fiber was based on maintaining a constant phase relation between the input phase and the phase of the received signal. An almost 40 times reduction of phase variation was achieved in this active control system using a 50/50 mirror for returning the optical signal from a receiving end to transmitting end [14]. In 1992, Kenneth designed and tested a prototype link of a 6.3GHz to 16GHz [4]. This year, Otoshi et al. tested a 12GHz fiber-optic system at NASA's Deep Space Network (DSN) station 13 to carry Ku-band (12GHz) signals from an antenna to a pedestal room. The tests performed only on the fiber-optic system portion of the overall test configuration showed that the 12GHz fiber-optic system had frequency stability of about 1.1×10^{-16} for 1000 second integration time for a nighttime run [5]. Sato et al. applied the optical fiber, which had been treated to reduce the thermal coefficient of delay and known as a phase stabilized optical fiber (PSOF), to the fiber-optic reference frequency distribution at NAO in 1992. The stability levels were about 7.0×10^{-15} at 5MHz in 1000 second averaging time [12]. In 1993, Calhoun applied this PSOF to a fiber-optic link at DSN. On-site measurements of this fiber-optic link alone showed the stability on the order of 10^{-16} at 1000 second integration time [6]. Johnson performed two-way tests on distribution systems employing state-of-the-art fiber optic transmitters and receivers under ideal, thermally stable laboratory conditions at JPL showing capability of achieving 1 part in 10^{-16} over 1000 second in 1993 [15]. Dragonette performed a study of signal quality maintained using inexpensive commercial transmitter/receiver

pairs at the Applied Physics Laboratory of Johns Hopkins University in 1993. The levels of performance achieved by these systems with commercial-based components were acceptable for reference frequency distribution [7]. Kotov evaluated an optical interferometric method that can provide optical phase shift proportional to RF signal phase shift transmitted through a fiber as an actively phase stabilizing system at the Technical University, Russia, in 1994. This system compensated the phase change of 12 degrees to 0.5 degrees at 15MHz [8].

To achieve the required ultra stable phase stability level of 1×10^{-16} in ASD for 1000 second averaging time for the frequency distribution, this thesis describes investigation and development of an ultra stable frequency distribution system of which response speed for phase fluctuations is fast. This ultra stable frequency distribution system applies a closed phase-locked loop with an optical fiber transmission line in which two optical carrier signals with different wavelengths are transmitted as a forward and a backward signal. The system consists of a local unit and a remote unit connected by a fiber optic cable. The PSOF is used for the signal transmission line. An optical signal, which is modulated by an injected reference signal, is transmitted to a remote unit through a fiber optic cable. An optical signal, which is modulated by the received reference signal in the remote unit, is sent back from the remote unit to the local unit through the same optical fiber cable. The delay at the remote end of the cable has exactly half the round trip delay. On the other hand, the phase difference between the transmitted and the returned signals at the transmitting end in the local unit is proportional to the round trip delay. Therefore, the phase at the remote end of the cable would be zero, when the phase difference between the transmitted and the returned signals from the remote unit, is adjusted by just a half of this round trip delay. A 1.55μm laser diode for the signal transmission from the local unit to the remote unit and a 1.31μm laser diode for the signal

transmission from the remote unit to the local unit are installed in the developed system. The phase difference between the transmitted and the returned signals is compensated by an optical delay control module (ODM). This is the first ODM application to be implemented for use in fiber optic frequency distribution system. This ODM induces no internal electronic noise in the fiber optic frequency distribution system.

The system noise level of a frequency stability measurement system is commonly the order of 10^{-16} for 1000 second integration time in ASD and this order is insufficient to measure the stability of developed ultra stable frequency distribution system with stability level of 10^{-17}. Thus, the frequency stability measurement system, of which system noise is the order of 10^{-17} for 1000 second integration time, has been designed this time. A vector voltmeter and a multimeter with long integration time in A/D conversion are first applied to achieve the lowest system noise in the frequency stability measurement system. The vector voltmeter outputs a DC analog signal proportional to compared phase difference between reference signal and test signal on direct analog output terminal. This is the first direct DC analog output usage of a vector voltmeter to be implemented for use in a frequency stability measurement system. The system noise level which is used for the laboratory measurement this time is better than any dual mixer time difference systems.

The stabilities of the developed ultra stable fiber optic frequency distribution system in ASD are 7.5×10^{-17} and 1.1×10^{-17} at 1000 second and 10,000 second averaging time respectively while the environmental temperature of the PSOF cable varies in the range of 10°C and at the rate of 10°C/12 hours. This system has the best stability in frequency distribution systems.

1.2 Outlines of the Thesis

In Chapter 2, statistics for frequency stability measurement are reviewed to evaluate phase stability in frequency distribution. Specifically, a method to evaluate phase stability of a frequency distribution system in a time domain is explained to apply the theory for evaluating the development system. Histories of development of fiber optic links for frequency distribution are also reviewed.

Chapter 3 reviews the fiber optic link systems applied in frequency distribution. The phase stabilized optical fiber and the two-way system are mentioned.

Chapter 4 presents development of the ultra stable fiber optic frequency distribution system. In this chapter, the stability requirement for a frequency distribution system is studied. The components for a fiber optic link are evaluated. Also, the developed system configuration is described.

The developed system is evaluated with laboratory measurements in Chapter 5 and the test results are also presented.

Chapter 6 concludes this thesis with discussions of the measured results, including some recommendations for the direction of further improvement and development.

CHAPTER 2

BASICS OF FREQUENCY DISTRIBUTION

2.1 Statistics for Frequency and Phase Stability Measurement

Allan studied and defined the characterization of frequency stability in the time domain and the frequency domain [16].

The output of an oscillator is defined as

$$V(t) = \left[V_0 + \varepsilon\ (t)\right]\sin\left(2\pi\ \nu_0 t + \phi(t)\right) \qquad (2\text{-}1)$$

where V_0 is the nominal peak output voltage, and ν_0 is the nominal frequency of the oscillator. Time-domain analysis is efficient for long-term performance evaluation like phase stability. Assuming that the time deviation is proportional to the phase deviation, the time deviation $x\ (t)$ of the signal given in the equation 2-1 can be expressed as

$$x\ (t) = \frac{\phi(t)}{2\pi\nu_0}\ . \qquad (2\text{-}2)$$

This relation can also be expressed as

$$x\ (t) = \int_0^t y(t')\ dt'$$

or

$$y(t) = \frac{dx(t)}{dt} \tag{2-3}$$

which relates frequency, time, and phase deviation.

The frequency deviations of precision signal sources are typically related in two categories: systematic and random deviations. The systematic deviations usually have the form of frequency and phase offset, frequency and phase drift, modulation sidebands, and dependence on environmental influences. The random deviations are categorically nondeterministic in character although the level would be deterministic and are often well described stochastically by power law spectral processes.

$$S_y(f) = \sum_{\alpha=-2}^{+2} h_\alpha f^\alpha \ . \tag{2-4}$$

In some cases f would be limited in bandwidth for particular values of α .

The classical variance diverges with the data length for $\alpha \leq -1$, and hence is not a good measure of a source's frequency stability. An IEEE subcommittee recommended a time-domain measure of frequency stability of a source which is convergent for all of the above kinds of power law spectra, in 1971.

$$\sigma_y^2(\tau) = 1/2 \left\langle \left(\bar{y}_{k+1} - \bar{y}_k \right)^2 \right\rangle \tag{2-5}$$

where the $\bar{y}_{k+1} - \bar{y}_k$ are adjacent measurements of the fractional frequency each averaged over a sample time τ . The expectation brackets "$\langle\ \rangle$" express taking all possible values of k which means infinite time average. This measure is called the "Allan variance".

For a finite set of N sequential adjacent samples of the frequency, each averaged over a sample time τ , $\sigma_y^2(\tau)$ is estimated as

$$\sigma_y^2(\tau) \cong \frac{1}{2(N-1)} \sum_{k=1}^{N-1} \left(\bar{y}_{k+1} - \bar{y}_k \right)^2 \ . \tag{2-6}$$

If the data are a set of $N+1$ time or phase deviation readings, then

$$\sigma_y^2(\tau) = \frac{1}{2\tau^2(N-1)} \sum_{k=1}^{N-1} \left(x_{k+2} - 2x_{k+1} + x_k\right)^2 \qquad (2\text{-}7)$$

since $\bar{y}_k = (x_{k+1} - x_k)/\tau$ where the interval of the x_k time deviation readings is τ. If a data set of $N+1$ time deviation readings, spaced by an interval τ_0, are measured and stored in a computer array, then $\sigma_y^2(\tau)$ for any $\tau = n\tau_0$, where $n = 1, 2, 3, \ldots, N/2$, would be calculated. In general, $\sigma_y^2(\tau)$ is expressed as

$$\sigma_y^2(\tau) = \frac{1}{2\tau^2(N+1-2n)} \sum_{k=1}^{N+1-2n} \left(x_{k+2n} - 2x_{k+n} + x_k\right)^2 . \qquad (2\text{-}8)$$

This equation gives high utilization and the best confidence of the estimate, which is also unbiased. This formula is called the "overlapping estimate" of the two-sample or Allan variance.

2.2 Relationship Between Frequency-Domain and Time-Domain Measures

The types of noise observed on the output signal of an oscillator can be represented most suitably by means of the spectral density $S_y(f)$ defined in the equation 2-4. This simple power-law model of the form and $S_y(f) = 0$ for $f > f_h$, where f_h denotes an ideally sharp upper cutoff frequency, are shown by experience to cover all actually known types of oscillators within the limits such as elimination of drift, etc [16]. The relation between Allan variance $\sigma_y^2(\tau)$ and a spectral density $S_y(f)$ is then shown as

$$\sigma_y^2(\tau) = 2\int_0^\infty S(f) \frac{\sin^4(\pi f\tau)}{(\pi f\tau)^2} df \ . \qquad (2\text{-}9)$$

When the power law spectral density of the noise in frequency domain is referred as flicker frequency modulation, the relation between $\sigma_y^2(\tau)$ and $S_y(f)$ is given as

$$S_y(f) = h_{-1} f^{-1} \tag{2-10}$$

and

$$\sigma_y^2(\tau) = 2 \cdot \ln(2) \cdot h_{-1} \ . \tag{2-11}$$

2.3 Relationship Between True Variance and Allan Variance

The true variance $I^2(\tau)$ and Allan variance $\sigma_y^2(\tau)$ can be calculated for the various types of noise described in section 2-1 and equation 2-4. For $\alpha = 1$ and 2, the variances converge only if a high-frequency cutoff f_h is specified. With this restriction, $\sigma_y^2(\tau)$ converges for all cases. $I(\tau)$ converges only for $\alpha \geq 0$. These functions are listed in Table 2-1 [18].

Table 2-1 Characteristics of Noise in Oscillators

Noise Type	$S_y(f)$	$S_\varphi(f)$	$\sigma_y^2(\tau)$	[a] μ	$I^2(\tau)$
White phase	$h_2 f^2$	$\nu_0^2 h_2$	$\frac{3h_2 f_h}{4\pi^2\tau^2}$ [b]	-2	$\frac{h_2 f_h}{2\pi^2\tau^2}$
Flicker phase	$h_1 f$	$\nu_0^2 \frac{h_1}{f}$	$\frac{3h_1}{4\pi^2\tau^2}\ln(2\pi f_h\tau)$	~-2	----
white frequency or random walk of phase	h_0	$\nu_0^2 \frac{h_0}{f^2}$	$\frac{h_0}{2\tau}$	-1	$\frac{h_0}{2\tau}$
Flicker frequency	$\frac{h_{-1}}{f}$	$\nu_0^2 \frac{h_{-1}}{f^3}$	$(2\ln 2)h_{-1}$	0	----
Random walk of frequency	$\frac{h_{-2}}{f^2}$	$\nu_0^2 \frac{h_{-2}}{f^4}$	$\frac{2\pi^2\tau}{3}h_{-2}$	1	----

[a] Power-law exponent of Allan variance: $\sigma_y^2(\tau) \propto \tau^\mu$.

[b] $2\pi f_h\tau >> 1$.

Except for the logarithmic dependence in this flicker phase noise, each noise component maps into a component of Allan variance of the form τ^μ. Thus, the total Allan variance is given as

$$\sigma_y^2(\tau) = \left[K_2^2 + K_1^2 \ln(2\pi f_h\tau)\right]\tau^{-2} + K_0^2\tau^{-1} + K_{-1}^2 + K_{-2}^2\tau, \qquad (2\text{-}12)$$

where the K's are constants. The subscripts of K correspond to the subscripts of h in Table 2-1. Both white phase and flicker phase noise result in $\mu \approx -2$, but these two

processes can be distinguished by varying f_h. For white phase and white frequency noise, the following relations are obtained

$$\sigma_y^2(\tau) = \frac{3}{2} I^2(\tau), \qquad \alpha = 2, \tag{2-13}$$

$$\sigma_y^2(\tau) = I^2(\tau), \qquad \alpha = 0. \tag{2-14}$$

2.4 Phase Stability Degradation by Discrete Noise in Frequency Synthesis

A phase stability of the signal, which is modulated by a discrete noise such as a power supply frequency in a frequency multiplication, is investigated by Yoshimura et al. [18].

There are two methods in frequency synthesis. The one is to use a phase locked oscillator and the other is the frequency mixing method. The method which uses a phase locked oscillator detects phase difference between synthesized output frequency and reference frequency by phase detector. A noise component in the error voltage of phase detector causes frequency modulation on the synthesized output frequency. The phase variation $\varphi(t)$ for one modulation frequency in frequency modulation is expressed as

$$\varphi(t) = \varphi_m \sin\left(2\pi f_m t + \theta\right), \tag{2-15}$$

where φ_m is modulation index and f_m is frequency of a modulation signal. Here θ denotes phase and is neglected because its value is constant. For several modulation frequencies, the equation 2-15 is rewritten as

$$\varphi(t) = \sum_i \varphi_{mi} \sin\left(2\pi f_{mi} t + \theta_i\right), \tag{2-16}$$

where i denotes the ith modulation frequency.

If the noise term, of which offset frequency is f_m, remaines in frequency mixing, modulated signal is expressed in the following formula.

$$\begin{aligned} V &= V_0 \sin 2\pi \nu_0 t + \nu_1 \cos 2\pi \left(\nu_0 + f_m\right) t \\ &= V_0 \left(1 - \varphi_m \sin 2\pi f_m t\right) \sin 2\pi \nu_0 t \\ &\quad + \nu_1 \cos 2\pi f_m t \cos 2\pi \nu_0 t \end{aligned} \tag{2-17}$$

where $\varphi_m \equiv \nu_1 / V_0 \ll 1$. The equation 2-17 is closely resembled as

$$V \approx V_0 \sin\left(2\pi \nu_0 t + \varphi(t)\right), \tag{2-18}$$

where

$$\begin{aligned} \varphi(t) &= \tan^{-1}\left(\varphi_m \cos 2\pi f_m t\right) \\ &\approx \varphi_m \cos 2\pi f_m t \end{aligned} \tag{2-19}$$

Thus, equations 2-15 and 2-19 have the same forms which are a trigonometrical function multiplied by modulation index. The difference of these two equations is that the noise term appears on both sides of the carrier in the equation 2-15 and the noise term appears on only the single side of carrier frequency in the equation 2-17. When the φ_m is considered to be the ratio of the amplitude of the modulation frequency to the one of the carrier signal, the function forms of a modulated carrier signal for the phase locked oscillator method and for the frequency mixing method becomes the same, while a carrier signal is a phase modulated by a discrete noise signal.

The normalized instantaneous frequency offset from the nominal value is designated as $y(t)$ in equation 2-3 and is defined as follows

$$y(t) = \frac{\nu_v}{\nu_0} = \frac{1}{2\pi \nu_0} \frac{d\varphi}{dt} \ . \tag{2-20}$$

Substituting the equation 2-15 to 2-20, $y(t)$ is given as

$$y(t) = \left(f_m / v_0\right)\varphi_m \cos 2\pi f_m t \tag{2-21}$$

Now, the autocorrelation of random process $g(t)$ is defined as follows,

$$R_g(\tau) = \left\langle g(t)g(t+\tau)\right\rangle . \tag{2-22}$$

Then the equation 2-21 is defined as

$$\begin{aligned} R_y(\tau) &= \left\langle y(t)y(t+\tau)\right\rangle \\ &= \left(f_m / v_0\right)^2 \varphi_m^2 \left\langle \cos 2\pi f_m t \cos 2\pi f_m (t+\tau)\right\rangle \\ &= \frac{1}{2}\left(f_m / v_0\right)^2 \varphi_m^2 \cos 2\pi f_m \tau \end{aligned} . \tag{2-23}$$

The single side power spectrum density $S_g(f)$ of $g(t)$ is defined according to the well-known Wiener-Khintchine relations, which is Fourier transformation of $R_g(t)$, as

$$S_g(f) = 4\int_0^\infty R_g(\tau)\cos 2\pi f\tau d\tau . \tag{2-24}$$

Substituting equation 2-23 to equation 2-24, $S_y(f)$ is rewritten as follows,

$$\begin{aligned} S_y(f) &= 2\varphi_m^2\left(\frac{f_m}{v_0}\right)^2 \int_0^\infty \cos 2\pi f_m \tau \cos 2\pi f\tau d\tau \\ &= \varphi_m^2\left(\frac{f_m}{v_0}\right)^2 \int_0^\infty [\cos 2\pi (f+f_m)\tau \\ &\qquad + \cos 2\pi (f-f_m)\tau] d\tau \\ &= \frac{1}{2}\varphi_m^2\left(\frac{f_m}{v_0}\right)^2 \left[\delta(f+f_m) + \delta(f-f_m)\right] \end{aligned} , \tag{2-25}$$

where $\delta(z) \equiv \frac{1}{\pi}\int_0^\infty \cos zt dt$ is Dirac's delta function and it is related as

$$\int_{-\infty}^{\infty} \delta(z)dz = 1,\ \delta(z) = 0\ (z \neq 0)\ . \tag{2-26}$$

The term of $\delta(f + f_m)$ is a component of $f = -f_m < 0$ in the equation 2-25 and is excluded due to the term being outside of definition area, which is $(f \geq 0)$, in $S_y(f)$. Thus the equation 2-25 is rewritten as

$$S_y(f) = 0.5\varphi_m^2(f_m / \nu_0)^2 \delta(f - f_m) \tag{2-27}$$

From the equations 2-16 and 2-23, the autocorrelation is given as

$$R_y(\tau) = \sum_i \left(\frac{f_{mi}}{\nu_0}\right)^2 \frac{\varphi_{mi}^2}{2} \cos 2\pi f_{mi}\tau\ . \tag{2-28}$$

Then the power spectrum density for several modulation frequencies is defined as

$$S_y(f) = \sum_i \frac{\varphi_{mi}^2}{2}\left(\frac{f_{mi}}{\nu_0}\right)^2 \delta(f - f_{mi})\ . \tag{2-29}$$

Allan variance is defined for the finite set of N sequential adjacent samples of the frequency. The generalized case is mentioned here. The first and second moments of the distribution $\bar{y}_k(t_k, \tau)$ are approximated by the mean value

$$\langle \bar{y}_k \rangle_N = \frac{1}{N}\sum_{k=1}^{N} \bar{y}_k\ , \tag{2-30}$$

where $t_{k+1} = t_k + T$; $k = 0,1,2,....$; T is the repetition interval for measurements of duration τ ; and t_0 is arbitrary. And the variance of the sample of N values

$$\sigma_y^2(N,T,\tau) = \frac{1}{N-1}\sum_{k=1}^{N}\left(\bar{y}_k - \langle \bar{y}_k \rangle_N\right)^2\ . \tag{2-31}$$

The broken brackets $\langle\ \rangle$ are used for practical cases where the number of samples are

finite but large enough for the error to be small. And $\left\langle \sigma_y^2(2,\tau,\tau) \right\rangle \equiv \sigma_y^2(\tau)$ is the special case called the Allan variance described in the section 2.1. The equation 2-31 is related with the spectral density $S_y(f)$ as

$$\left\langle \sigma_y^2(N,T,\tau) \right\rangle = \frac{N}{N-1} \int_0^\infty S_y(f) \left| H(f) \right|^2 df \,, \tag{2-32}$$

where

$$\left| H(f) \right|^2 = \frac{\sin^2 \pi f\tau}{(\pi f\tau)^2} \left(1 - \frac{\sin^2 \pi rf\tau N}{N^2 \sin^2 \pi rf\tau} \right) \tag{2-33}$$

and

$$r = T / \tau \,. \tag{2-34}$$

The equation 2-9 in the section 2.2 is given substituting $N = 2$ and $r = 1$ to the equations 2-32 to 2-34 as the special case.

Substituting the equation 2-27 to the equations 2-32 to 2-34 and considering the relation of the equation 2-26, the relation between the variance and the power spectrum density of the modulation frequency is given as

$$\left\langle \sigma_y^2(N,T,\tau) \right\rangle = \frac{N}{(N-1)} \frac{\varphi_m^2}{2} \left(\frac{f_m}{\nu_0} \right)^2 \frac{\sin^2 u}{u} \left[1 - \frac{\sin^2 Nru}{N^2 \sin^2 ru} \right] \tag{2-35}$$

where $u \equiv \pi f_m \tau_0$. When the modulation frequency is multiple, the relation is shown as

$$\left\langle \sigma_y^2(N,T,\tau)\right\rangle = \frac{N}{(N-1)}\sum_i \frac{\varphi_{mi}^2}{2}\left(\frac{f_{mi}}{\nu_0}\right)^2 \frac{\sin^2 u_i}{u_i}\left[1-\frac{\sin^2 Nru_i}{N^2\sin ru_i}\right] \tag{2-36}$$

where $u_i \equiv \pi f_{mi}\tau_0$. As the special case, $N = \infty$ and $N = 2$, the equation 2-35 gives the following standard deviations,

$$\left\langle \sigma_y^2(\infty,T,\tau)\right\rangle^{\frac{1}{2}} = \frac{\varphi_m}{\sqrt{2}}\left(\frac{f_m}{\nu_0}\right)\frac{|\sin u|}{u} \tag{2-37}$$

$$\left\langle \sigma_y^2(2,T,\tau)\right\rangle^{\frac{1}{2}} = \varphi_m\left(\frac{f_m}{\nu_0}\right)\frac{|\sin u||\sin ru|}{u} \tag{2-38}$$

$$\sigma_y(\tau) = \varphi_m\left(\frac{f_m}{\nu_0}\right)\left[\frac{\sin^2 u}{u}\right]. \tag{2-39}$$

For the multiplex modulation frequencies, the standard deviations are given while adding each modulation frequency component as shown in equation 2-36.

The characteristics of the terms $|\sin u|/u$ and $(\sin^2 u)/u$ are shown in Fig. 2-1.

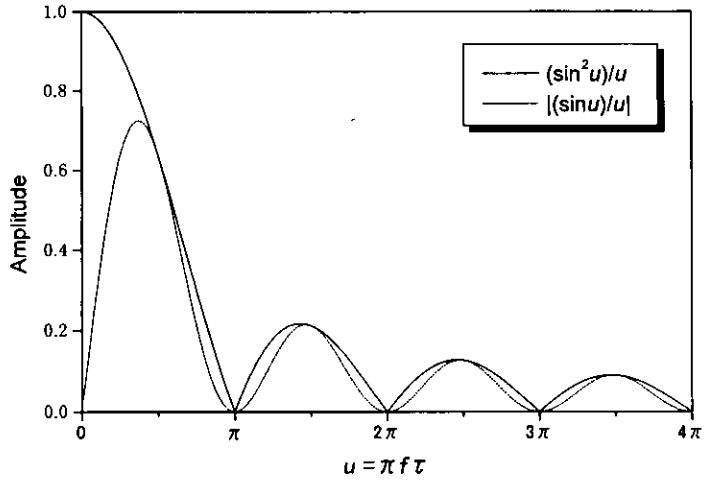

Figure 2-1 Frequency window of a discrete noise spectrum

2.5 Histories in development of Fiber Optic Link for Frequency Distribution

Lutes installed a 3km experimental multimode optical fiber link operating at an 850nm wavelength at Jet Propulsion Laboratory (JPL) in 1979. This system was to be used in the development of ultra-stable frequency and timing distribution systems. The link achieved a stability of 4×10^{-15} for 100 second integration time at 100MHz. The stability was limited by the optical transmitter and receivers. Delay changes as a result of bending multimode fibers were nonreciprocal under some circumstances, and excessively large [1].

Since the first fiber optic link was applied in frequency distribution at JPL, it became apparent that it would be necessary to use single-mode fibers operating at 1.3μm wavelength to distribute stable high frequencies. This was because of the lower loss, wider bandwidth and theoretically reduced delay change with bending which were associated with single-mode fiber operating at this wavelength. Lutes et al. developed a single-mode fiber capability at JPL in 1986. After the experiment was completed, the link was set up for one-way distribution of the signal between two stations and was used as the station reference for a successful connected element interferometry experiment. The two station references were coherent with better than 1.5×10^{-15} for 1000 second integration time at 100MHz because of the improved signal-to-noise ratio (SNR) and stability of the link over the one way path length [2].

While developing a fiber optic reference frequency distribution system, to which semiconductor laser transmitters were applied by Lutes at JPL in 1989, it was found that changes in reflection from the fiber back into the laser diode at transmitting end cause delay variations across the laser which may be as great as

100ps. It was shown that an optical isolation of the laser on the order of 60 dB could reduce such changes to less than 0.03 ps [3]. Lutes also applied this optical isolator to the 850m length fiber-optic frequency reference distribution link achieving about 2.5×10^{-15} for 1000 second integration time at 100MHz in 1989 [13].

The advantage of using fiber-optic cable as the transmission medium is that the superior performances of the optical components make it quite practical to transmit the signal simultaneously in both directions in the same fiber. This proves to be a key factor in actively stabilizing the distribution system.

Primas et al. tested an active stabilization of a fiber-optic frequency distribution system at JPL in 1989. The method for actively controlling the phase variations in the fiber was based keeping the phase difference constant between the output and returne signal. An almost 40 times reduction of phase variation was achieved in this active control system using a 50/50 mirror for returning the optical signal from a receiving end to transmitting end [14].

The single-mode fiber itself is capable of supporting bandwidth to at least 100GHz over distances of 1km, while the remaining active optelectronic elements have much lower bandwidth restrictions.

In 1992, the bandwidth limitations for the different optoelectronic components, that were commercially available, were given by laser diode; 18GHz, modulator; 18GHz, detector; 60GHz. Based on these limits, Kenneth designed and tested a prototype link of a 6.3GHz to 16GHz [4]. In the same year, Otoshi et al. tested a 12GHz fiber-optic system at NASA's Deep Space Network (DSN) station 13 to carry Ku-band (12GHz) signals from an antenna to a pedestal room. The tests performed only on the fiber-optic system portion of the overall test configuration showed that the 12GHz fiber-optic system had frequency stability of about 1.1×10^{-16} for 1000 second integration time for a nighttime run [5].

Sato et al. applied the optical fiber, which had been treated to reduce the thermal coefficient of delay and known as a phase stabilized optical fiber (PSOF), to the fiber-optic reference frequency distribution at NAO in 1992. The stability levels were about 7.0×10^{-15} at 5MHz in 1000 second averaging time [12]. In 1993, Calhoun applied this PSOF to a fiber-optic link at DSN. On-site measurements of this fiber-optic link alone showed the stability on the order of 10^{-16} at 1000 second integration time [6].

Johnson performed two-way tests on distribution systems employing state-of the-art-fiber optic transmitters and receivers under ideal, thermally stable laboratory conditions at JPL showing capability of achieving 1 part in 10^{-16} over 1000 second in 1993 [15].

Reference signal distribution has been effectively disseminated using high-quality fiber-optic distribution systems. The stability of signals distributed by these systems is excellent, but the cost of these systems makes them unavailable to many potential users.

Thus, Dragonette performed a study of signal quality maintained using inexpensive commercial transmitter/receiver pairs at the Applied Physics Laboratory of Johns Hopkins University in 1993. Seven different transmitter/receiver pairs obtained from four different manufactures had been thoroughly tested using a 5MHz sinusoid derived from a precision, temperature-controlled, crystal-controlled oscillator. The electrical signal output from each fiber-optic receiver was tested for spectral purity, single-sideband phase noise, and AM noise. The levels of performance achieved by these systems with commercial-based components was acceptable for reference frequency distribution [7].

Kotov evaluated an optical interferometric method that can provide optical phase shift proportional to RF signal phase shift transmitted through a fiber as an

actively phase stabilizing system at the Technical University, Russia, in 1994. This system compensated the phase change of 12 degrees to 0.5 degrees at 15MHz [8].

CHAPTER 3

FIBER OPTIC LINK SYSTEMS IN FREQUENCY DISTRIBUTION

3.1 Phase Stabilized Optical Fiber

Thermal coefficient of transmission delay time (TCD) for an optical fiber was reduced to zero at 0°C by Sumitomo Electric Industries, Ltd. in 1987 [11].

The TCD time for an optical fiber is expressed as

$$\frac{d\tau}{dt} = \tau\left[\frac{1}{N}\frac{dN}{dT} + \frac{1}{L}\frac{dL}{dT}\right], \tag{3-1}$$

where τ, N and L represent the interval time, refractive index of silica glass and the length of an optical fiber. The first term indicates the temperature dependence of refractive index of silica glass, which is an intrinsic value in the optical fiber. The value of this term is approximately +30 ps/km/°C, or 6 ppm/°C for total transmission delay time. In order to reduce and finally to eliminate the TCD of the optical fiber, the second term, the thermal expansion coefficient of the coated fiber, must be of a negative value and cancel the first term as well.

The thermal expansion coefficient α of a coated fiber is given by,

$$\alpha = \frac{1}{L}\frac{dL}{dT} = \frac{\sum_i k_i E_i S_i}{\sum_i E_i S_i} \tag{3-2}$$

where k_i , E_i , and S_i represent the thermal expansion coefficient, Young's modulus and cross section of i-th material, respectively.

Generally, the tight coated optical fibers are doubly coated with soft resins (primary coating resins: silicone, UV curable resin) and thermoplastic resin (secondary coating resins: nylon, elastmer etc,). When the product of Young's modulus and the cross section of primary coating resin ($E_{pri} \times S_{pri}$) are much smaller than the others in equation 3-2, this term can be neglected. Then equation 3-2 is expressed as

$$\alpha = \frac{\sum_i k_i E_i S_i}{\sum_i E_i S_i} = \frac{k_g E_g S_g + k_{\sec} E_{\sec} S_{\sec}}{E_g S_g + E_{\sec} S_{\sec}} \tag{3-3}$$

where g denotes glass fiber and sec denotes secondary coating resin. In order to give zero thermal coefficient of transmission delay time, the following equation must be satisfied.

$$\left(1 + \frac{1}{N}\frac{dN}{d\varepsilon}\right)\alpha_{\frac{d\tau}{dT}=0} = -\frac{1}{N}\frac{dN}{dT} + \frac{1}{N}\frac{dN}{d\varepsilon}k_g, \tag{3-4}$$

where ε and $\frac{1}{N}\frac{dN}{d\varepsilon}$ represents stress and the stress dependence of refractive index of silica glass. From the equations 3-3 and 3-4, the relation of k_{sec} versus E_{sec} and S_{sec} can be given by,

$$k_{\sec}\frac{d\tau}{dT} = \alpha_{\frac{d\tau}{dt}=0} - \frac{\left(\alpha_{\frac{d\tau}{dT}=0} - k_g\right)E_g S_g}{E_{\sec} S_{\sec}} \tag{3-5}$$

where $\alpha_{\frac{d\tau}{dT}=0} = \dfrac{-\frac{1}{N}\frac{dN}{dT} + \frac{1}{N}\frac{dN}{d\varepsilon}k_g}{1+\frac{1}{N}\frac{dN}{d\varepsilon}}$

when putting typical values 7100 for E_g, 0.123 for S_g, 6×10^{-7} for k_g, 6.5×10^{-6} for $\frac{1}{N}\frac{dN}{dT}$ and 0.2 for $\frac{1}{N}\frac{dN}{d\varepsilon}$, the equation (3-6) is given,

$$k_{\sec\frac{d\tau}{dT}=0} = -8.28\times10^{-6} - 7.73\times10^{-4}\left(E_{\sec}S_{\sec}\right)^{-1}, \qquad (3\text{-}6)$$

When an optical fiber is coated with a material whose Young's modulus is 2000 kg/mm^2 and its coating diameter is 0.8 mm, theoretical value of $k_{\sec\frac{d\tau}{dT}=0}$ is calculated as -9.31×10^{-6}/°C.

The value of this thermal expansion coefficient of the coated fiber depends on the value of the thermal expansion coefficient in both primary and secondary coating. A secondary coating resin having a negative thermal expansion coefficient is required in tight coated optical fibers.

Thermotropic hard liquid crystal polymer (LCP) that had a negative thermal coefficient (-7 ~-9×10^{-6} /°C) as the secondary coating resin was selected for zero TCD optical fiber. This zero TCD optical fiber cable is called a phase stabilized optical fiber (PSOF). Fig. 3-1 shows the cross section of an LCP coated optical fiber.

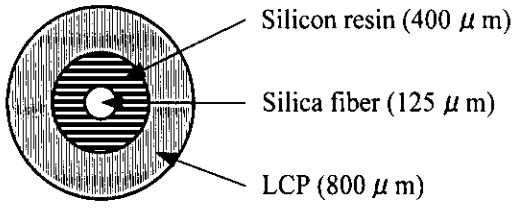

Figure 3-1 Cross section of LCP coated single mode fiber

3.2 Two-way Systems

The method for actively controlling the phase variation in the fiber is based on maintaining a constant phase relation between the input phase and the phase of the transmitted signal. The transmitted optical signal should be returned from the far end to the reference end to compare the phase between the signals transmitted and returned as shown in Fig. 3-2. A signal passing through the fiber-optic cable in both directions experiences identical delay in each of the two directions. The midpoint of the signal is at the far end of the cable and experiences exactly half the round-trip delay. As long as the transmitted and returned signals propagate in the same cable, the phase at the remote end is independent of phase variation in the medium shown in Fig. 3-2.

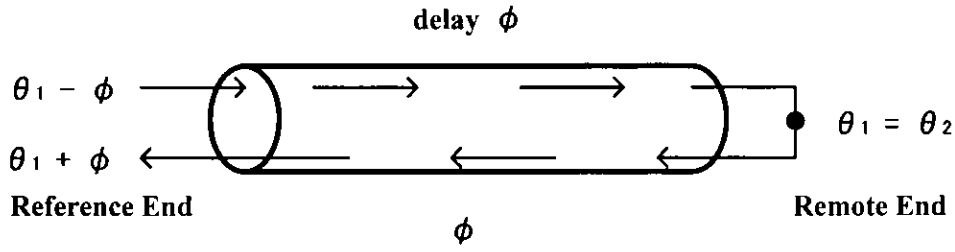

$$\theta_2 = (\theta_1 - \phi) + \frac{(\theta_1 + \phi) - (\theta_1 - \phi)}{2} = \theta_1$$

Figure 3-2 Phase conjugation relations between input and output signals

Two methods have been suggested to return the signals from the remote end to the reference end.

3.2.1 50/50 Mirror System

Primas et al. designed the two-way fiber-optic link to produce the actively controlling method [14]. The method was to apply a 50/50 mirror at the far end.

The 50/50 mirror at the remote unit reflected half the optical signal back toward the reference end while the other half passed through the mirror. The block diagram of system is shown in Fig. 3-3 .

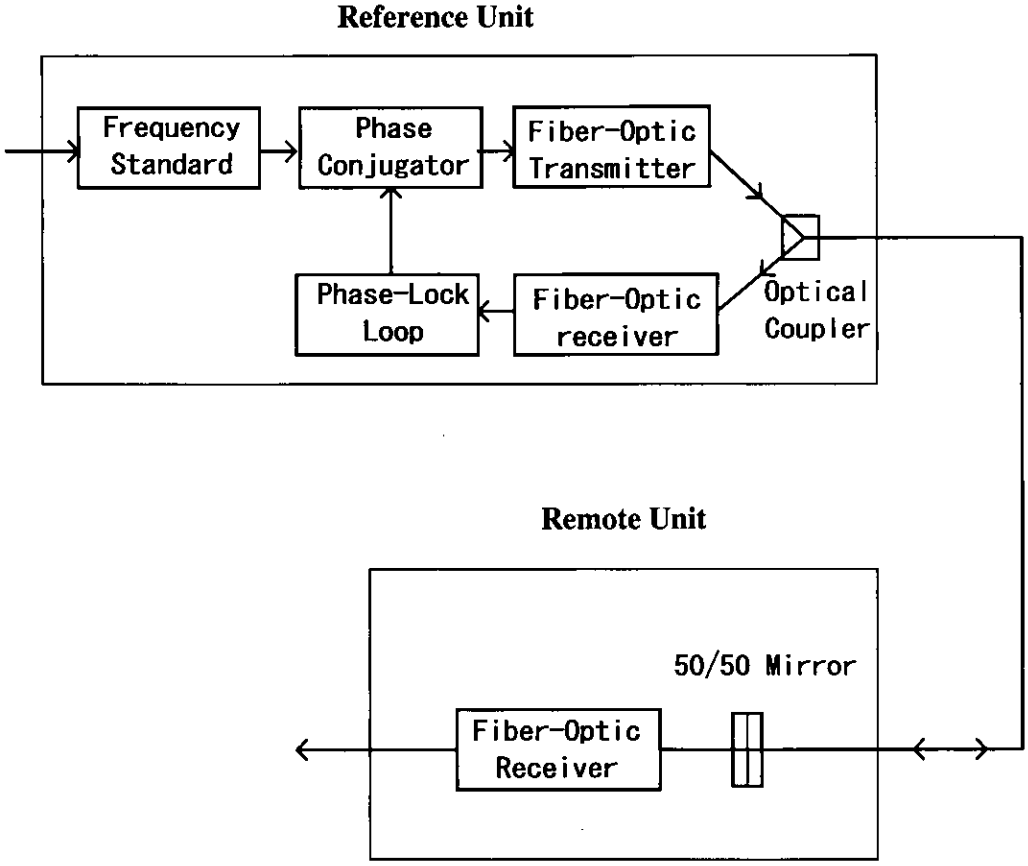

Figure 3-3 Application of 50/50 mirror for returning signal from far end to reference end

One of the disadvantage of this 50/50 mirror was that the mirror weakens the return signal. The optical leakage of the transmitting reference signal through the coupler entered directly into the reference unit receiver and cause cross modulation of the leakage signal and the reflected signal.

The phase variation caused by the difference between the return signal and the leakage signal is

$$\Phi = \arctan\left[10^{-R/20}\right] \tag{3-7}$$

where Φ is the phase variation in degrees and R is the power ratio of the leakage signal to the returned signal in dB. If the return signal is 40 dB greater than the leakage signal, the resulting phase variations exceeds 0.57 degrees. Thus, this 50/50 mirror reflection method makes it theoretically difficult to reduce this cross modulation in general.

3.2.2 Two Transmitter and Receiver Pairs System

The other method is to provide individual transmitter and receiver pairs for each of the forward and backward signals.

This method was evaluated by Johnson using the system shown as Fig. 3-4 [15].

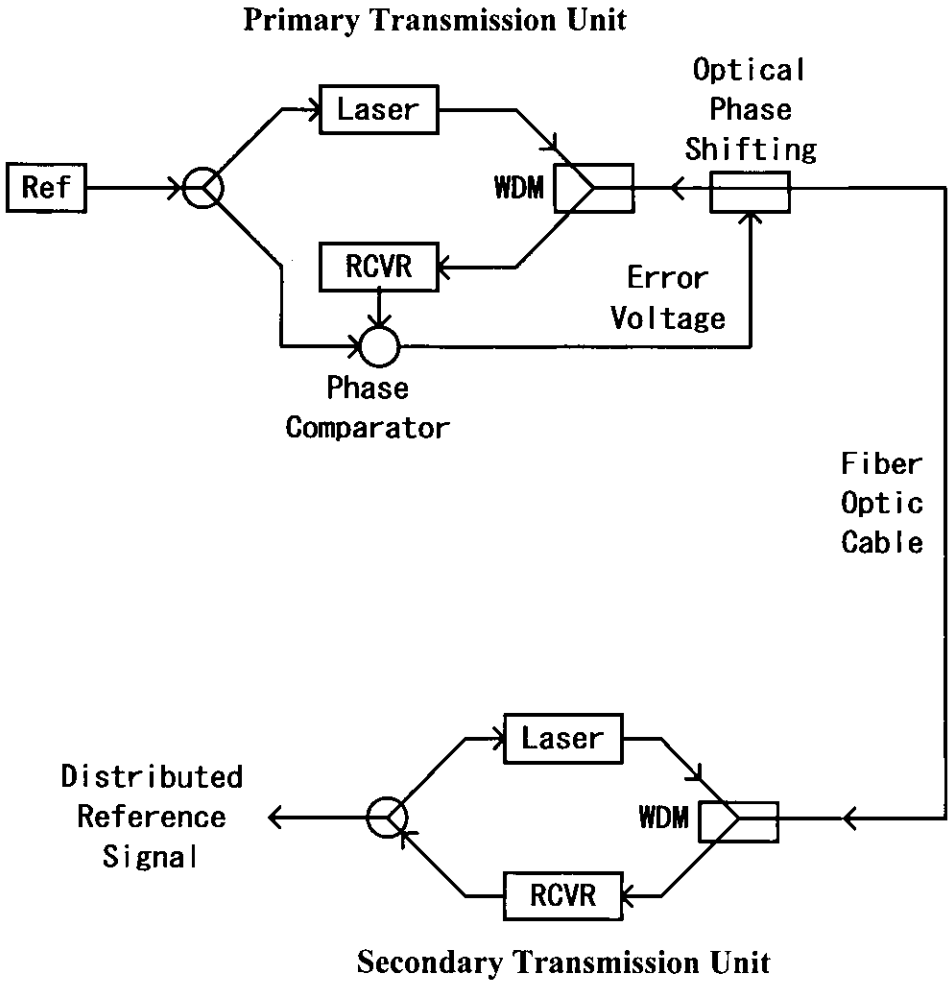

Figure 3-4 Block diagram of a fiber optic frequency distribution system employing two transmitter and receiver pairs.

In this case the primary transmission unit transmitted the reference frequency through the optical fiber, while the secondary transmission unit returned the far end signal back to the reference end through the same optical fiber path. To isolate the forward and backward transmissions, the primary and secondary links were supported by two different optical wavelengths and signals generated by each system were routed to different receivers by use of wavelength division multiplexers at each end of the common transmission path. A thermally controlled fiber delay coil is used to compensate for induced phase variations in this system.

3.2.3 Bandwidth in Phase Stabilization

In both 50/50 mirror system and two transmitter and receiver pair system, an optical feedback technique was employed to compensate phase delay variation in an optical fiber cable and to supply a stable reference frequency at the far end. The resulting feedback signal then drove stabilizer circuitry which in turn adjusted the phase of the transmitting reference frequency at the transmitting end to actively compensate for the phase delay variations. A voltage controlled oscillator or phase modulator was employed as narrow-band stabilization method to shift the required phase angle.

An alternative wide-band method which provided a phase compensation for reference frequency signals in wide bandwidth and involved manipulating only the optical signal itself, was also tested [15]. Two advantages of the wide-band system over narrow-band designs are (1) that it provides phase compensation for all transmitted frequencies, and (2) the compensation is applied after the optical interface rather than electronically ahead of it as in narrow-band designs. In the wide-band method, the reference frequency signal which is transmitted from the

reference end to far end is not electrically manipulated in phase adjustment. Thus, no phase stability degradation will be adopted to the reference frequency signal itself.

CHAPTER 4

DEVELOPMENT OF THE SYSTEM

4.1 Stability Requirements

4.1.1 Stability Requirement in Frequency Standard

One of the purposes in developing the ultra stable frequency distribution system is to apply the system for distribution of a reference frequency supplied by an atomic frequency standard. The frequency stability level of a hydrogen maser frequency standard is around (2 to 3)$\times 10^{-15}$ for the integration time of 1000 second in ASD.

A liner ion trap frequency standard was researched and developed lately [9]. This frequency standard was based on the 40.5GHz ground state hyperfine transition of ^{199}Hg ions confined in a trap to allow for long interrogation times and high atomic line Q. Continuous operation was practical using a ^{202}Hg lamp to generate 194.2nm radiation for atomic selection and helium buffer gas for ion cooling. The liner ion trap provided a way to increase the detected fluorescence signal to noise without increasing the second order Doppler shift. The developed mercury linear ion trap frequency standard could achieve a short term stability performance of $\sigma_y(\tau) = 2 \times 10^{-14} / \tau^{1/2}$ when it is operated with an appropriate local oscillator. The

long term stability design goal was to achieve an average frequency drift rate of less than 1×10^{-16} /day, which corresponds to one thirtieth in hydrogen masers. The typical stabilities of these atomic frequency standards are shown in Fig. 4-1.

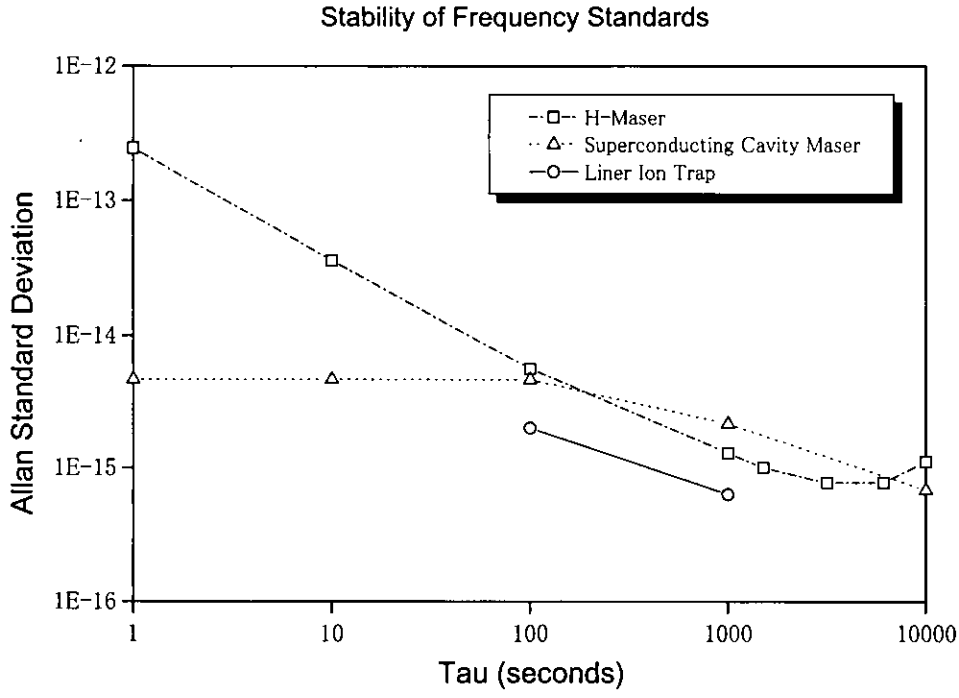

Figure 4-1 Stability of frequency standards

According to the previous review, the phase stability level of 1×10^{-16} in ASD at 1000 second averaging time is required for a frequency distribution system of the frequency standards.

4.1.2 Stability Requirement in Differential VLBI

In the differential VLBI observations, the delay path length for a target source is measured relative to the delay path length for a reference source to reduce the variations of the path length caused by the atmospheric fluctuation [10]. The accuracy of the relative delay path length required in this measurement is less than 0.1 mm RMS. In VLBI, the delay path length is estimated as the phase difference between a pair of antennas. The accuracy of the measured phase difference is necessary to be kept less than 1 degree RMS, 3 degrees RMS and 5 degrees RMS at 8GHz, 22GHz and 43GHz, which are observation frequencies of the differential VLBI, respectively. The phase errors are caused not only by atmospheric fluctuations, but also from various parts of the observation instruments such as a gravitational deformation of an antenna, a front-end receiver, a local oscillator for a down conversion, a signal transmission line for IF signal, a reference signal transmission line for a local oscillator, a delay calibration unit and an analog-to-digital (A/D) converter in a VLBI sampler unit. Since the total phase error is given by the root-sum-square (RSS) of the phase variations caused in the individual parts of the instruments and the atmosphere, the allowed value of the phase error in the frequency distribution system is assigned 1/3 of the total phase errors, that is less than 0.3 degrees at 8GHz.

According to the equation 2-13, while assuming the white phase noise and

$\langle \bar{y}_k \rangle = 0$, the RMS phase variation $\langle \Delta\phi^2 \rangle^{\frac{1}{2}}$ increases with the time T according to an equation,

$$\langle \Delta\phi^2 \rangle^{\frac{1}{2}} = \sqrt{\frac{2}{3}}\sigma_y(T)\omega T \quad , \tag{4-1}$$

where σ_y is the ASD of the frequency distribution system, and ω is the angular frequency of the distributed signal [12][16]. Therefore the stability value in ASD as 1.2×10^{-13} and as 1.2×10^{-16} for averaging times of 1 and 1000 second at 8GHz respectively are obtained in the worst case. In the frequency distribution system, the transmitting frequency of the reference signal is 1.4GHz. The allowed value of stability is established as 5×10^{-14} in ASD for one second averaging time at the distributing frequency of 1.4GHz, that is 2.4 times better than the estimated value for the observing frequency at 8GHz, to restrict one second short period noise of each component in the developed frequency distribution system. According to these considerations, the stability value in ASD as 1×10^{-16} in 1000 second averaging time at the distributing frequency of 1.4GHz is also adopted as the allowed value.

4.2 Idea of System

To meet the requiment of the stability, the active phase comparison design with two way method reviewed in section 3.2 is employed.

4.2.1 Frequency Distribution System

Fig. 4-2 shows the basic idea of the developed actively stabilized frequency distribution system. The system consists of a local unit and a remote unit connected

by a fiber optic cable. An optical carrier signal, which is modulated by an injected reference signal, is transmitted to a remote unit through a fiber optic cable. An optical carrier signal, which is modulated by the received reference signal in the remote unit, is sent back from the remote unit to the local unit through the same fiber optic cable. The delay at the remote end of the cable has exactly half the round trip delay. On the other hand, the phase difference between the transmitted and the returned signals at the transmitting end in the local unit is proportional to the round trip delay. Therefore, the phase at the remote end of the cable would be zero when the phase difference between the transmitted and the received signals, which is returned from the remote unit, at the transmitting end of the cable in the local unit is adjusted by just a half of this round trip delay.

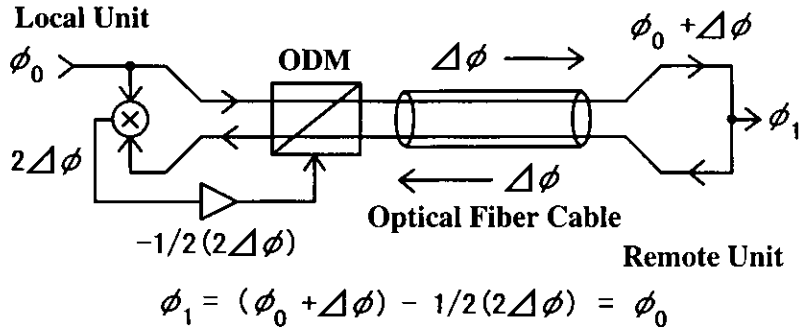

Figure 4-2 Conceptual model for a closed phase-lock loop using a single fiber optic frequency transmission line.

Previously, two different methods were applied for returning the optical carrier

signals from the remote unit to the local unit. One method applied a 50/50 mirror [14], and the other method applied different optical carriers which were a 1.30μm and a 1.55μm for forward and backward signals respectively [15], as reviewed in the section 3.2. In the former method, the optical carrier signal transmitted from the local unit was directly sent back from the remote unit to the local unit. And the degradation of the SNR occurred due to weak returned optical carrier signals [14]. On the other hand, a phase delay difference between two optical carrier wave lengths occurred in the latter method.

The phase delay difference is estimated assuming that a 1.55μm and a 1.33μm optical carrier waves are used for forward and backward signals. A phase delay difference between the 1.33μm and the 1.55μm optical carrier waves is caused by the difference of a reflection index between these two optical carrier waves. The difference of the phase delay per unit length Δt_0 is given as $\Delta n/c$, where Δn is the difference of the reflection index between two optical carries and c is a speed of light in a vacuum. For the 1.33μm and the 1.55μm optical carriers, the difference of the reflection index is about 0.004 in optical glass, and Δt_0 is estimated as 13ns/km. This phase delay is constant and compensated in a phase coincide loop. The temperature dependency of this reflection index is typically of the order of 10^{-6}/°C in optical glass, and the temperature dependency for the difference of the reflection index between the 1.33μm and the 1.55μm optical carriers is 0.004×10^{-6}/°C which corresponds to the phase variation of about 0.01ps/°C/km. The allowed value for phase error in the VLBI observation is assumed as 0.3 degrees at 8GHz that corresponds to 0.1ps at 8GHz. The phase variations caused by the difference of the reflection index are quite small compared with the stability requirement. Therefore, the two-way system in which a 1.55μm laser diode for the signal transmission from the local unit to the remote unit and a 1.31μm laser diode for the signal transmission

from the remote unit to the local unit are installed.

As reviewed in section 3.2.3, the wide-band system has two advantages over narrow-band designs. The one is that it provides phase compensation for all transmitted frequencies. The other is that the compensation is applied after the optical interface rather than electronically ahead of the optical interface in narrow-band designs. In the wide-band method, the reference frequency signal which is transmitted from the reference end to far end is not electrically manipulated in phase adjustment. Thus, no phase stability degradation will be adopted to the reference frequency signal itself.

To implement this wide-band method, thermally controlled phase compensator was tested by Johnson [15] and concluded as the compensation provided by the thermal stabilizer design was relatively slow, and thus disturbances varying for less than several tens of seconds cannot be properly compensated. The response for the disturbances is important for VLBI observations because of antenna slewing. To improve the response speed in the development this time, an optical delay control module (ODM) is employed. The phase comparison between the transmitted and the returned signals is done by an ODM because it will induce no internal electronic noise. This module is designed not to yield the differential dispersion effect for the operating optical wavelengths. The response speed of this optical delay module is less than 100ms for the delay range from 0 ps to 100ps, and the delay resolution is less than 0.1 ps.

4.2.2 Phase Measurement System

A dual mixer time difference system (DMTD) has been frequently used for precise frequency stability measurements because of having no dead-time errors and

a simple measurement system, but the estimation of its measurement precision has been still discussed by many researchers. In the DMTD method, a frequency signal of interest f_0 and a reference signal $f_0+\delta f$ are frequency converted to low frequency f_0-f_0' by each frequency converter drived at the same local frequency f_0'. The difference between the zero crossing times of two low frequency signals is measured. It is evident that the measurement error decreases to $\Delta t \times (f_0 - f_0') / (f_0 \times \tau)$ from $\Delta t / \tau$, when Δt and τ are a time measurement error of a measuring instrument (time intervasl counter) and integration time respectively.

A time interval counter for general use has the time measurement error Δt of 1×10^{-6} to 20×10^{-6}, and $f_0 - f_0'$ is usually 1Hz or so. Assuming f_0 to be 10MHz and 100 second of τ, the frequency stability is estimated to be about 1×10^{-16}. Unfortunatelly this stability is not enough for our measurement system which requires 10^{-17}. For this reason, the new measurement system with the stability level of 10^{-17} for the integration time of 1000 second has been developed.

The new system consists of a vector voltmeter, a digital multimeter and a data acquisition computer. A direct analog output from the vector voltmeter is directly proportional to the phase difference between the frequency signal of interest and a reference one. It is sampled by the digital multimeter and averaged by the data acquisition computer.

This measurement system has great advantages not only in the excellent stability but also in the estimation of the obtained stability. According to the equation 2-31 in the section 2.4, the Allan variance assumes that the repitation interval of a measurement sampling and the duration of one sampling are the same. The DMTD method which uses a time interval counter for phase difference measurement can not implement this assumption properly because the counter detects instantaneous phenomenon of the phase as zero crossing point. However, this

theoretical assumption can be realized properly applying a digital multimeter with long integration time in A/D conversion to measure a signal from a direct analog output of a vector volt meter. The integration time in A/D converter is equivalent to the duration of the equation 2-31.

4.3 System Design with Fiber Optic Link

There are many parameters which characterize the performance of a fiber optic link. The major parameters that relate with SNR and phase variations, when the link is used for a frequency distribution system, are discussed [26].

4.3.1 Link Gain

The RF loss in an optical link is a function of the laser quantum efficiency, the laser to fiber coupling efficiency, the fiber loss, the photodiode responsivity and the ratio of the output to input impedance.

The quantum efficiency and the fiber coupling efficiency are combined in a single specification called the modulation gain. With coupling of 15%, the modulation gain is typically 0.04mW/mA. That is, when operated above the threshold current, 0.04mW of optical power will be launched into the fiber for every milliampere of input current supplied to the laser.

This DC modulation gain will determine the average coupled laser light power. However, overall link gain will be a function of frequency and so the effective modulation gain is also a function of frequency. The delivered power gain of the link can be written in terms of the input and output currents.

$$G = \frac{i_{out}^2 R_L}{i_{in}^2 R_{in}} \tag{4-2}$$

$$G_{dB} = 10\log\left(\frac{i_{out}^2 R_L}{i_{in}^2 R_{in}}\right) \tag{4-3}$$

where R_L is output load resistance and R_{IN} is input resistance of the link. Assuming the resistances are matched to 50 Ω at the input and the output, $R_L = R_{IN} = 50\ \Omega$. Then,

$$G_{dB} = 10\log\left(\frac{i_{out}^2}{i_{in}^2}\right) = 20\log\left(\frac{i_{out}}{i_{in}}\right) \tag{4-4}$$

The laser and photodiode are operated in their linear region as shown in Fig. 4-3.

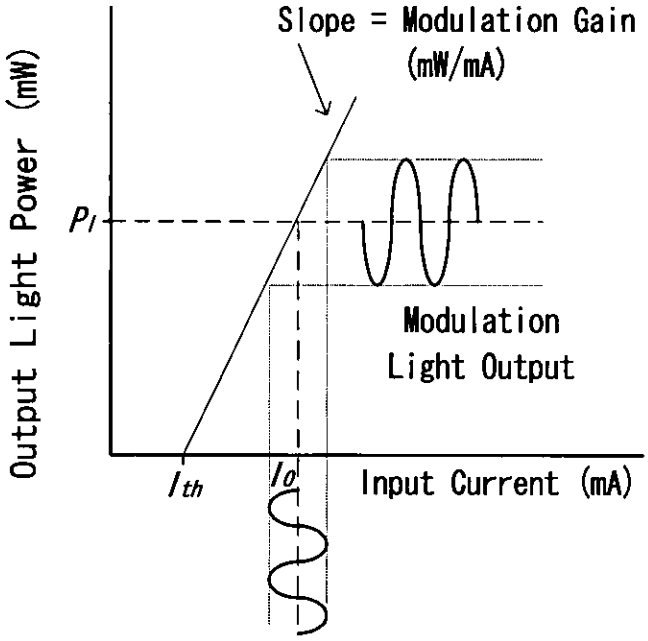

Figure 4-3 Laser L-I Curve

The factor which converts input current to laser optical power coupled into the fiber is the modulation gain, M (mW/mA). The optical loss in the fiber and the connectors is given by L_{opt}. The factor which converts incident optical power to photodiode output current is the responsivity, r (mA/mW). Finally, the photodiode current is delivered to the parallel combination of the photodiode module output resistance, R_o, and the local resistance, R_L. Each notations are shown in Fig. 4-4.

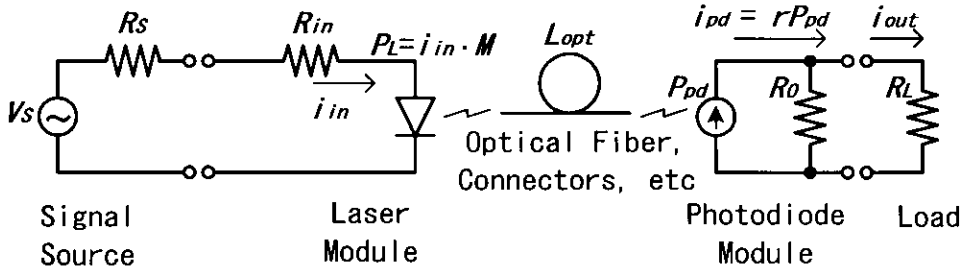

Figure 4-4 Equivalent of a Simplified Laser Link Circuit for Link Gain Calculation

Therefore,

$$i_{out} = \left(\frac{R_o r M}{R_o + R_L}\right) r \left(\frac{M}{L_{opt}}\right) i_{in} \quad . \tag{4-5}$$

The optical loss is usually given in dB as

$$L_{dB} = 10 \log L_{opt} \tag{4-6}$$

From equations 4-5 and 4-6, equation 4-4 is rewritten as

$$G = 20\log\left(\frac{R_o rM}{R_o + R_L}\right) - 2L_{dB} \ . \tag{4-7}$$

Taking account of the input and load impedance, the equation is given as

$$G = \left[\left(\frac{R_o rM}{R_o + R_L}\right)\left(\frac{rM}{L_{opt}}\right)\right]^2 \frac{R_L}{R_{in}} \ . \tag{4-8}$$

or, the equation is written in dB

$$G = 20\log\left(\frac{R_o rM}{R_o + R_L}\right) - 2L_{dB} + 10\log\left(\frac{R_L}{R_{in}}\right). \tag{4-9}$$

4.3.2 Relative Intensity Noise (RIN) and Equivalent Input Noise (EIN)

For analog communications, a laser is DC biased in the middle of its linear region that is, at some current I above I_{th}, the threshold current shown as Fig. 4-3. When so biased the laser emits light with average intensity P_o, the power is considered to be average because even if the biasing current were perfectly constant with time, the laser output light exhibits small intensity fluctuations. Thus, a relative intensity noise (RIN) is defined as the ratio of the square mean amplitude of those fluctuations to the square of the averaging intensity level.

$$RIN = \frac{\langle \Delta\ P^2 \rangle}{P_o^2} \quad \text{(1 Hz Bandwidth)} \tag{4-10}$$

Now, the laser converts input current to output optical power. Since the laser is operated in the liner region of the L-I curve as shown in Fig. 4-3, this conversion is a constant - namely, with the modulation gain, M.

Therefore RIN is given as

$$RIN = \frac{\langle \Delta I^2 \rangle M^2(f)}{(I - I_{th})^2 M^2(0)} \quad , \tag{4-11}$$

where $< \Delta I^2 >$ is the mean square of the input current fluctuations that would produce the observed output light intensity fluctuations if the laser itself were noiseless. Also, the frequency dependence of the effective modulation gain is indicated. The denominator has the DC modulation gain or light vs. current slope since it relates to the average optical output power coupled into the fiber. In the numerator the modulation gain is a function of frequency. The frequency dependence of the modulation gain could be found by measuring the link gain as a function of frequency using a photodiode with a known responsivity, r, connected to the laser with a fixed optical loss, L_{opt} and using equation 4-8 to compute $M(f) = M(0)$. Then

$$RIN = \frac{\langle \Delta I^2 \rangle}{(I - I_{th})^2} \tag{4-12}$$

for $M(f) = M(0)$.

The RF input circuit including the laser diode has an input impedance R_i. The current fluctuation $< \Delta I^2 >$ through R_i give an electrical noise power which is called the laser equivalent input noise (EIN). Thus,

$$EIN \text{ (Watts)} = < \Delta I^2 > R_i \tag{4-13}$$

where $< \Delta I^2 >$ is in units of A^2. Therefore, the EIN is given as

$$EIN = RIN(I - I_{th})^2 R_i . \tag{4-14}$$

4.3.3 Optical Components Characteristics

4.3.3.1 Laser Diode Module

NEC laser diode model NDL7610PA and model NDL7710PA are selected for 1.31μm and 1.55μm wavelengths respectively. The outline of the package is shown in Fig. 4-5.

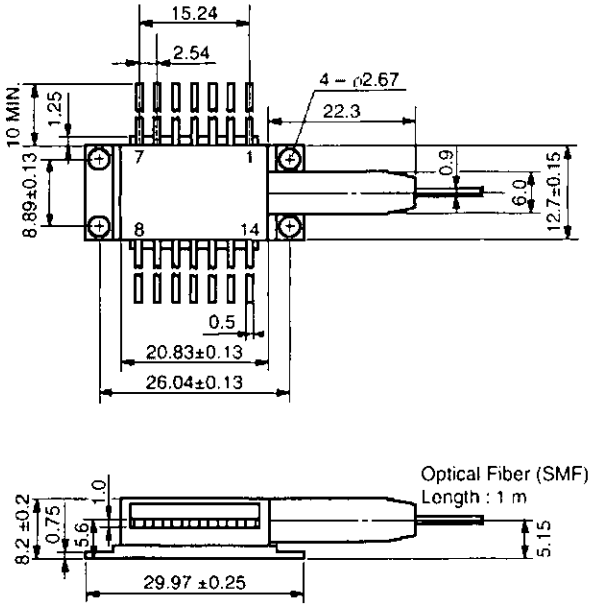

Figure 4-5 Package outline of NDL7610P and NDL7710PA laser diodes

These models are butterfly package modules with a single mode fiber for 2.5

Gb/s optical fiber communication systems. The laser diode has a multiple quantum well (MQW) structure and phase-shifted distributed feed-back (DFB). This laser diode can achieve stable dynamic single longitudinal mode operation under high speed modulation. It consists of an InGaAs monitor photo diode, thermistor, thermo-electric cooler, optical isolator and impedance matching circuit. YAG laser welding techniques are utilized to achieve stable optical coupling over wide operating temperature range.

When the output power to an optical fiber cable P_f is assumed to be 2 mW, $I_F = I_{th}$ +30mA, RIN = -150dB/Hz, and input impedance $R_{in} = 25\Omega$ referred to the data sheet of these models [27][28]. Then, from equation 4-14, EIN is given as EIN $= 1\times10^{-15}\times(0.03)^2\times25 = 2.25\times10^{-17}$ W/Hz = -136.5 dBm/Hz. An output power P_C of modulated carrier with modulation index m is given as

$$P_C = P_O \cdot m \cdot \frac{1}{\sqrt{2}} \quad . \tag{4-15}$$

P_C is -1.5dBm when P_O and m are 2 mW and 0.5 respectively. The unit of EIN is W/Hz or dBm/Hz, and EIN time frequency bandwidth f_C is the total power of input noise in the laser diode module. The carrier to noise ratio (C/N) is then defined as P_C / (EIN $\times f_C$). The C/N of these laser modules is calculated as 39 dB when f_C is 4GHz referring to the data sheet, while the optical isolation of these laser diode modules is 40 dB typically.

4.3.3.2 Photo Diode Module

An NEC model NDL5422P photo diode is selected for receiving 1.31μm and 1.55μm wavelength laser signals. This model is InGaAs PIN photodiode with 6 pin butterfly package module containing a silicon pre-amplifier IC. The outline of the

package is shown in Fig. 4-6.

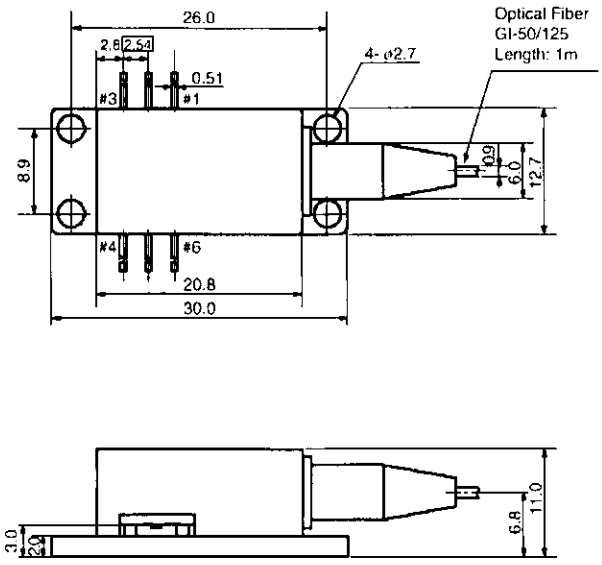

Figure 4-6 Package outline of NDL5422P photo diode

This is designed as an optical receiver for 2.5 Gb/s fiber optic communications system. YAG laser welding techniques are utilized to achieve stable optical coupling over wide operating temperature range from -40°C to +70°C.

The noise power of a photo diode is defined as

$$P_N = I_n^2 R_O \ . \tag{4-16}$$

When received optical power P_r = 1 mW, modulation index m = 0.5, impedance R_O = 50 Ω, equivalent noise current I_n is $9.0pA/\sqrt{Hz}$ referring to the data sheet [29].

Then P_N is calculated as -174 dBm/Hz. The output power P_S of a photo diode is written as

$$P_S = \left(I_S \cdot Z_t\right)^2 / R_O \tag{4-17}$$

where Z_t is transimpedance, and R_O is output impedance. P_S is calculated as -8.4dBm while parameters I_S = 0.28mA, Z_t =300 Ω, and R_O =50 Ω according to the result of experiment and data sheet. Finally the carrier to noise ratio (C/N) is then defined as $P_S / (P_N \times f_C)$. Thus, the C/N of the photo diode modules is calculated as 69.6 dB when f_C is 4GHz referring to the data sheet.

4.3.3.3 Optical Delay Control Module

The ODM is a key component of the ultra stable fiber optic frequency distribution system. Santec corporation model ODL-610 is selected as optical delay control module. The outline of the package is shown in Fig. 4-7.

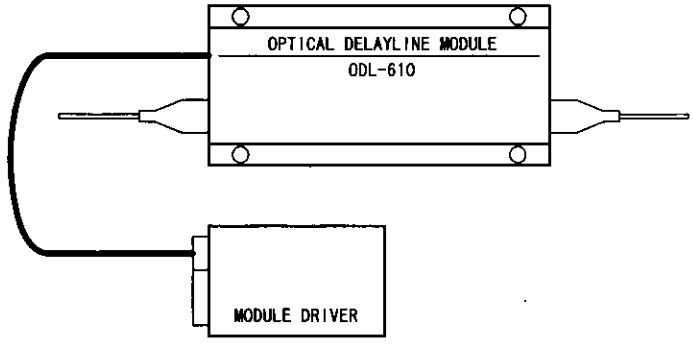

Figure 4-7 Package outline of ODL-610 optical delay control module

This module has a potential to vary optical delay over a wide range from 0 psec to 130 psec and the delay can be precisely controlled by changing the distance between two high efficiency fiber collimators using a reflection mirror. The specifications of this model are shown in the Table 4-1 [30]. The allowed value for phase error in the VLBI observation is assumed as 0.3 degrees at 8GHz that corresponds to 0.1ps at 8GHz.

Table 4-1 Specifications of Model ODL-610 Optical Delay Control Module

Wavelength	1.55μm/1.31μm
Delay	0 - 130 psec
Resolution	< 0.1 psec
Insertion Loss (IL)	1.5 - 2.5 (0 - 130 psec) dB
Isolation in Reflection	> 40 dB
Tuning Speed	< 100 msec (0 - 100 psec)

4.3.3.4 Phase Comparator

An R&K model M-14LL double balanced mixer is selected as a phase comparator. The frequency ranges are 800MHz to 1600MHz for RF&LO signals and DC to 500MHz for an IF signal, respectively [31]. The maximum conversion losses are 9.0dB for 800MHz to 1200MHz and 10.0dB for 1200MHz to 1600MHz at LO drive level of +7dBm. The isolations between IF and LO is 20dB for 800MHz to

1200MHz and 17dB for 1200MHz to 1600MHz. The maximum peak RF input power is 500mW. The impedance at all ports is 50Ω.

The minimum detectable phase angle which is proportional to the phase difference between the signals injected into RF and LO ports while this module is applied as a phase comparator is estimated as follows. If the output signal level is +4dBm when the input level and the actual conversion loss are assumed to be +10dBm and 6dB, respectively. Then the voltage of the output signal is calculated to be 0.35V for the output impedance of 50Ω. The peak voltage is then given as $0.35\times\sqrt{2}$ V, so that output voltage V is described as $V = 0.35\times\sqrt{2}\sin\phi$ when the phase difference ϕ is around zero. The minimum detectable phase angle is then calculated as $\phi = \sin^{-1}\left(1\times10^{-3}/0.35\times\sqrt{2}\right) = 0.12\ ^\circ$ when the minimum detectable voltage of the multimeter is assumed to be 1mV. As shown in section 4.1.2, the total phase error in this frequency distribution system is required to be less than 0.3° at 8GHz which corresponds to 0.05° at 1.4GHz. This requirement of the total phase error suggests that the multimeter should have the measurement accuracy of 0.4mV.

4.4 Improvement of ODM Driver for Less Backlash

The ODM utilized for the ultra stable fiber optic frequency distribution system was proved to have a backlash characteristic in delay change to its driving voltage while the system was being assembled.

The ODM module used for the system is the model ODL-610 manufactured by Santec Co. Ltd. Its delay resolution is less than 0.1 psec which is equal to required phase accuracy of 0.05° at 1.4GHz. It was found that the actual ODM assembled in

this system did not move smoothly and showed the action like backlash. The step angle by the backlash reached about 1° at 1.4GHz. In order to reduce this backlash characteristic of the ODM, we had to develop a unique electrical driving circuit with a digital servo loop. This digital servo loop driving circuit puts an AC bias upon the driving voltage for the ODM. The frequency of the AC bias is 100Hz and the voltage is 80mV to 120mV. The block diagram of this digital servo loop driving circuit is shown in Fig. 4-8. Fig. 4-9 shows an improved backlash characteristic. The backlash in hysteresis would be estimated as 0.1 degrees at 1.4GHz in Fig. 4-9. This value 0.1 degrees is twice as much as the delay resolution of the model ODL-610 and is one third of the stability requirement which is 0.3 degrees at 8GHz mentioned in section 4.1.

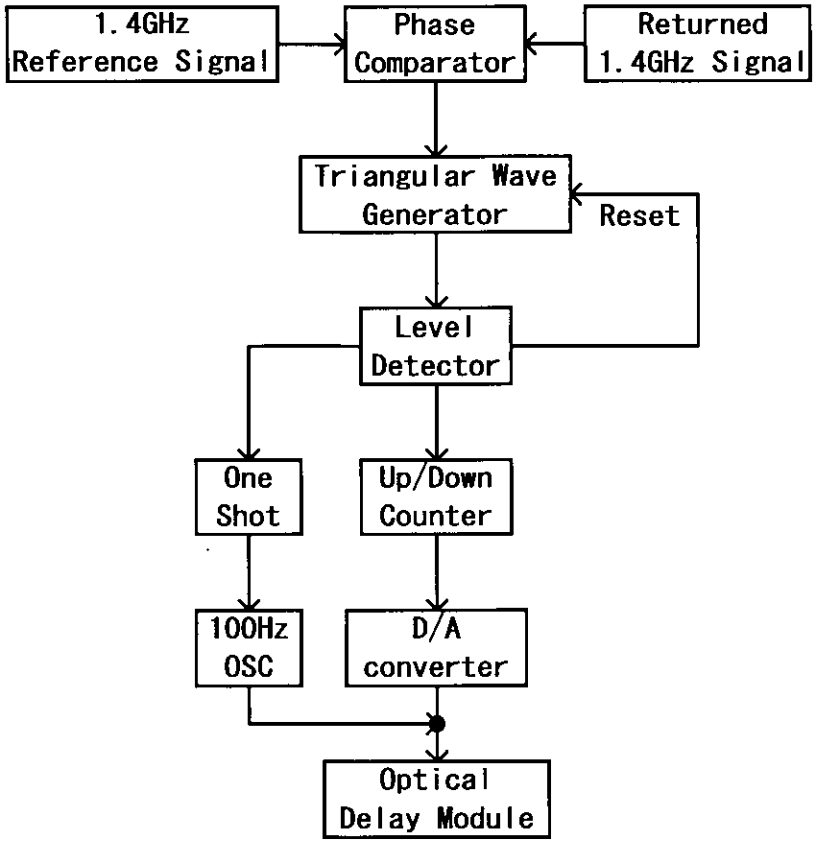

Figure 4-8 Block Diagram of Digital Servo Loop Driving Circuit

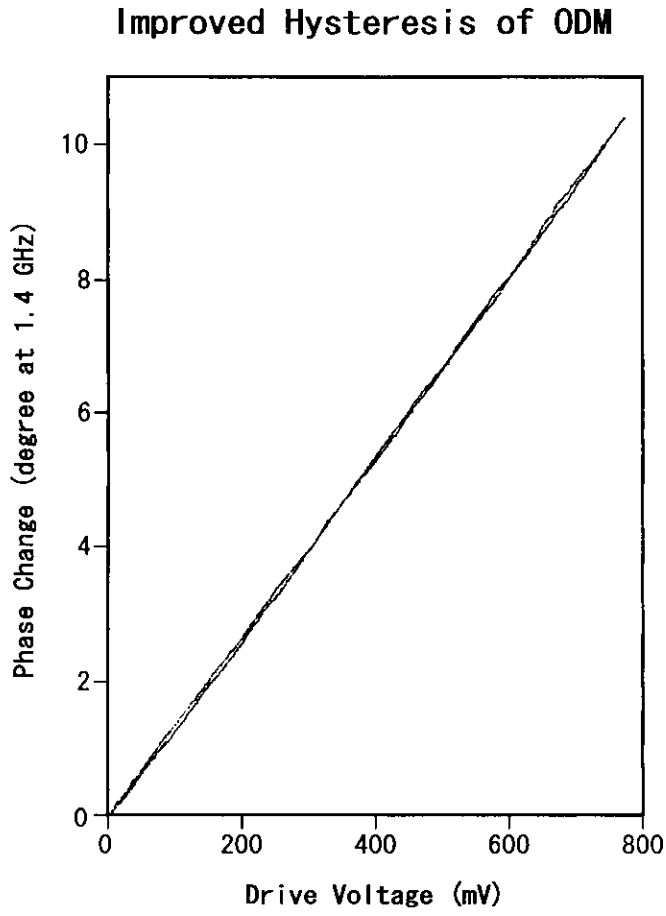

Figure 4-9 Improved backlash characteristic of the ODM

4.5 Outline of the System

The ultra stable frequency distribution system consists of a control unit located at an antenna control room and an antenna unit located at a remote receiver room on an antenna. A block diagram of this system is shown in Fig.4-10.

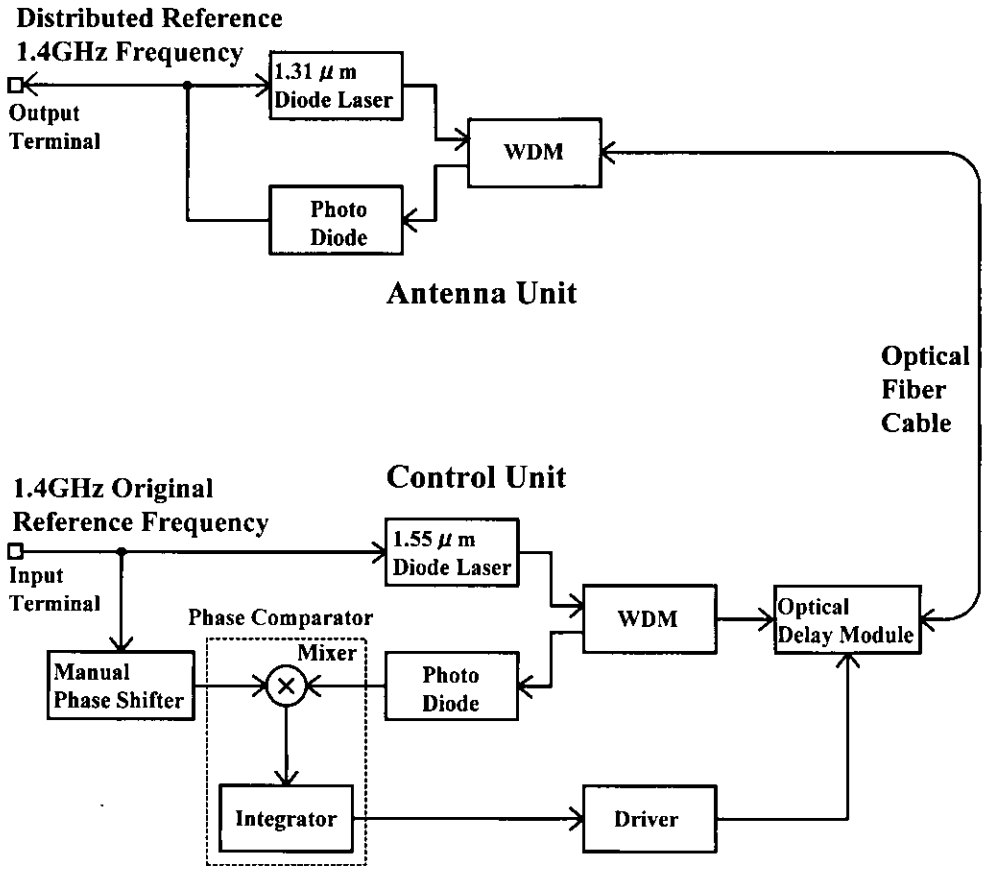

Figure 4-10 Block diagram of the developed ultra stable frequency distribution system

The control unit is composed of a 1.55μm laser diode, a WDM, an ODM, a 1.31μm photo diode, a manual phase shifter and a phase comparator. The antenna unit is composed of a 1.31μm laser diode, a 1.55μm photo diode and a WDM.

A 1.4GHz reference signal supplied from a Hydrogen Maser frequency standard is converted to an optical carrier signal with the 1.55μm laser diode module in the control unit, and transmitted to the antenna unit via the WDM, the ODM and the PSOF cable. At the antenna unit, the 1.4GHz reference signal is demodulated from a 1.55μm optical carrier signal. The 1.4GHz RF signal demodulated in the antenna unit is converted to a 1.31μm optical carrier signal and sent back to the control unit thorough the same PSOF cable. The returned optical carrier signal is fed to the photo diode via the ODM and the WDM, and is demodulated to a 1.4GHz RF signal. The phase difference between the returned RF signal and the 1.4GHz reference supplied from the Hydrogen Maser frequency standard is compared with the phase comparator. The ODM is controlled by the output DC signal of the phase comparator to compensate the phase difference.

The developed ultra stable fiber optic frequency distribution system is shown in Fig. 4-11. The upper is the control unit and the lower is the antenna unit.

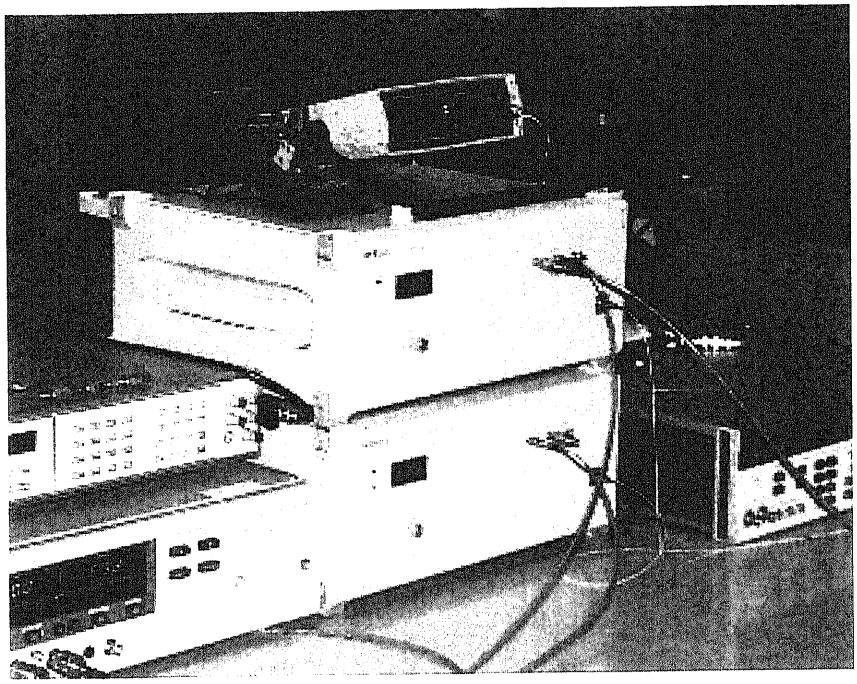

Figure 4-11 Developed ultra stable fiber optic frequency distribution system (middle row). The upper is the control unit and the lower is the antenna unit.

CHAPTER 5

LABORATORY MEASUREMENT

OF THE SYSTEM

5.1 Measurement System

The phase stability of the ultra stable frequency distribution system is measured by the system shown in Fig. 5-1.

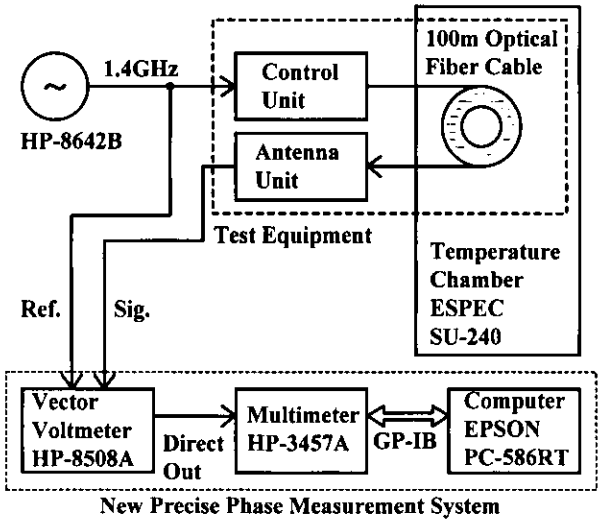

Figure 5-1 Block diagram of the phase stability measurement system

The measurement system consists of a 1.4GHz signal source, a temperature chamber and the new precise phase measurement equipment. The new precise phase measurement equipment is composed of a vector voltmeter, a digital multimeter and a personal computer with GP-IB interface. The test equipment is installed between the 1.4GHz signal source and the vector voltmeter. In the vector voltmeter, the phase of the signal through the test equipment is compared with that of the signal directly fed from the 1.4GHz signal source. The PSOF cable of 100m long connecting the control unit to the antenna unit of the test equipment is placed in the temperature chamber, while the temperature in the chamber is varied for simulating a daily environmental temperature variation.

5.1.1 Specification of Vector Volt Meter

The vector voltmeter utilized in the measurement system is Hewlett Packard model 8508A with 50 ohm input module. Specifications are listed in Appendix B.

There is very important specification in this HP-8508A vector voltmeter to make the frequency stability measurement system as state-of-the-art specification. The HP-8508A outputs DC analog voltage proportional to phase difference between a reference signal and received signal. The direct analog output provides continuous phase difference through an 800Hz low-pass filter.

5.1.2 Specification of Digital Multimeter

The digital multimeter which is utilized in the measurement system is Hewlett Packard model 3457. Model 3457 converts an analog DC voltage to digital one. Once the signal is converted to digital form, it can be displayed and sent over the GP-

IB bus.

The input signals are converted to digital values by model 3457's A/D converter. The A/D converter is responsible for many of model 3457's operating characteristics. These characteristics include AC line rejection (ability to reject signals at the power supply frequency from measurements), measurement speed, resolution, and accuracy. When power is supplied, model 3457 measures the power supply frequency such as 50Hz, 60Hz, or 400Hz automatically. The A/D converter then sets its reference frequency to match the measured frequency, or in the 400Hz case, a subharmonic of that frequency. This allows model 3457 to reject unexpected signals of power supply frequency from measurements when the integral number of power line cycles (1, 10, or 100) is specified for the integration time. The reference frequency also affects the measurement speed.

The integration time is the duration of sampling. This time is specified in number of power line cycles as a parameter of the command named NPLC. The range is available from 0.0005 to 100 power line period. For example, the period of a 50Hz power line is 1/50=20 msec. When the power line period is set to 0.1, the integration time is 20 msec×0.1=2 msec.

The resolution is determined by the integration time of the A/D converter. When a certain resolution is specified, an integration time is specified indirectly. Typically, the NPLC command should be used to select the required amount of normal mode rejection, and the % resolution parameter to select the required resolution.

The relationship between the NPLC, the resolution parameter (as a percentage of full scale), the maximum number of digits available, and the AC line rejection are shown in Table 5-1.

Table 5-1 A/D Converter Relationships

Power Line Period	Percentage of Full Scale	Maximum Number of Digits	AC Line Rejection
0.0005	0.033%	3.5	0dB
0.005	0.0033%	4.5	0dB
0.1	0.00033%	5.5	0dB
1	0.000033%	6.5	60dB
10	-	7.5*	80dB
100	-	7.5*	90dB

* Extra Resolution

5.1.3 Test Configuration in Laboratory

The test equipment and the measurement system are placed in the basement of the Mizusawa Astrogeodynamics Observatory, where the room temperature is kept within less than ±0.5 °C for a day.

The test configuration is shown in Fig. 5-2. The left most unit on the desk is the computer for quick viewing of measuring ASD and data logging. The upper in second row from left side is the multimeter. The lower in second row from left side is the vector voltmeter. The upper in third row from left side is the control unit of the ultra stable fiber optic frequency distribution system. The lower in third row from left side is the antenna unit of the system. The unit in fourth row is the 1.4GHz signal generator. The right most on the desk is the spectrum analyzer. The right most of the Fig. 5-2 is the temperature chamber in which the PSOF cable is located.

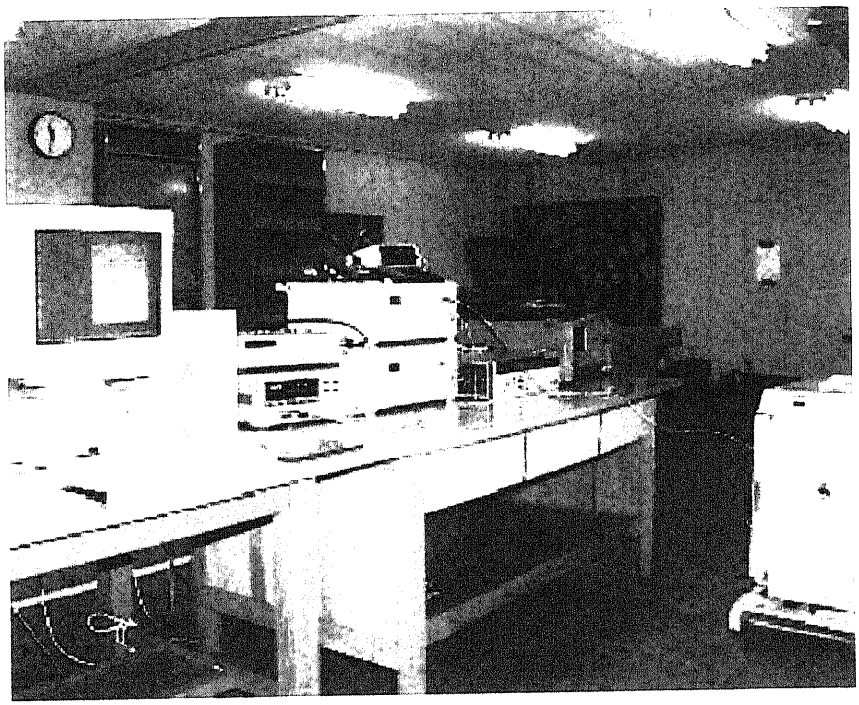

Figure 5-2 Test configuration at a laboratory

As stated in section 4.1.2, the allowed value of the phase error for the frequency distribution system in VLBI observation is estimated less than 0.3 degrees at 8GHz. This estimated value corresponds to 0.05 degrees at 1.4GHz. The display resolution of the vector voltmeter is 0.1 degrees, so that it does not satisfy our requirement of 0.05° at 1.4GHz. To improve the resolution, signals from a direct analog output were measured.

The direct analog output of the vector voltmeter, which is proportional to a phase difference between a reference signal and a signal through the test equipment, is sampled by the multimeter. The resolution can be selected to less than 0.4mV which correspond to 0.05° at 1.4GHz. The sampled data are transferred to the personal computer through the GP-IB interface. This sampled data are stored in a file. The ASD of the measured phase difference is calculated every 10 second for a quick look by the personal computer.

5.1.4 Characteristic of Measurement System

Phase stability is related to an integration time of each sampled data. This integration time corresponds to the sample time of the A/D converter in the multimeter. The phase stability is measured under the condition where the closed phase-lock loop is enabled and the sample time is one second, by setting the integration time of the multimeter to 200ms, 20ms, 2ms, 0.1ms and 0.01ms, which corresponds to the cut-off frequencies of 5Hz, 50Hz, 500Hz, 10kHz and 100kHz respectively. The results are shown Fig. 5-3.

The Fig. 5-3 shows that the ASD is proportional to the cut-off frequency when the frequency is lower than 500Hz, while it is constant above 500Hz. This result reflects the characteristics of an 800Hz lowpass filter installed in the vector

voltmeter. From this analysis, the integration time of 200ms, which corresponds to 5Hz in the cut-off frequency was selected.

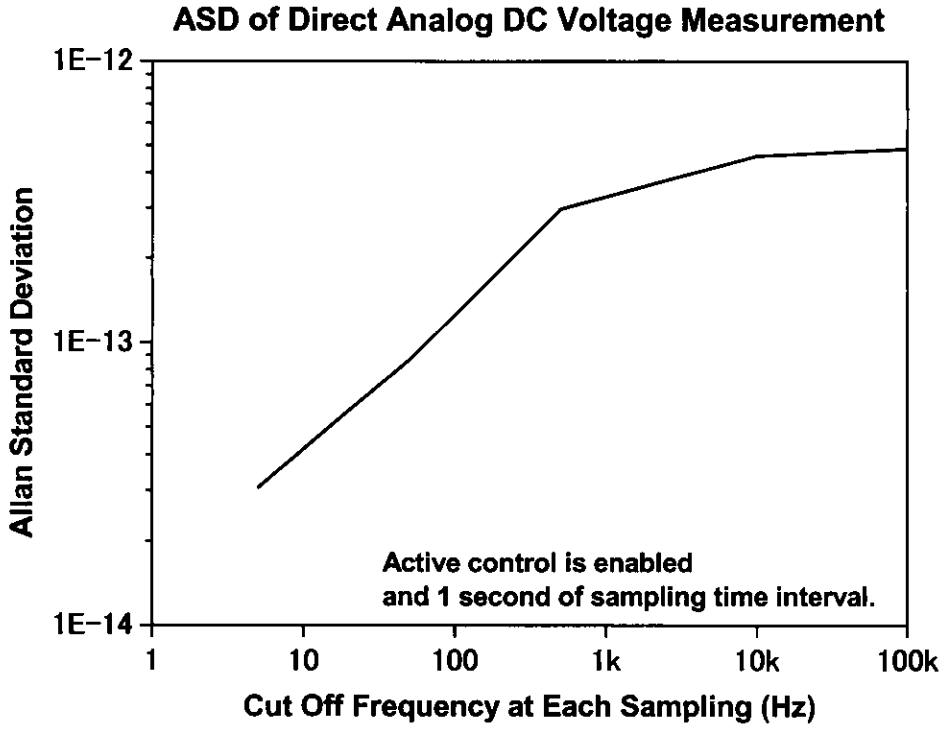

Figure 5-3 ASD of direct analog DC voltage measurement with 800Hz filter in new precise phase measurement system.

5.1.5 Calculation Program of Allan Standard Deviation

A voltage reading, which is proportional to a phase variation, is sampled at 1 second interval and stored into a hard disk of a personal computer. ASD of the tested fiber optic distribution system is calculated and displayed every 10 samples of phase variation measurement on a CRT display. The purpose of this simultaneous calculation is for a quick look to evaluate the measured data in advance. A calculation program was prepared to analyze the measured results in batch mode. The theory of this calculation is based on the equation 2-8. The program is written in BASIC language to execute in a personal computer and is listed in appendix A. The calculated results by this program is analyzed mainly by the software named Origin which is produced by Microcal Corporation and runs on windows 95&98 operating system.

5.1.6 System Noise Level of Measurement System

The system noise level of the measurement system is shown in Fig. 5-4 together with other phase stability measurement results.

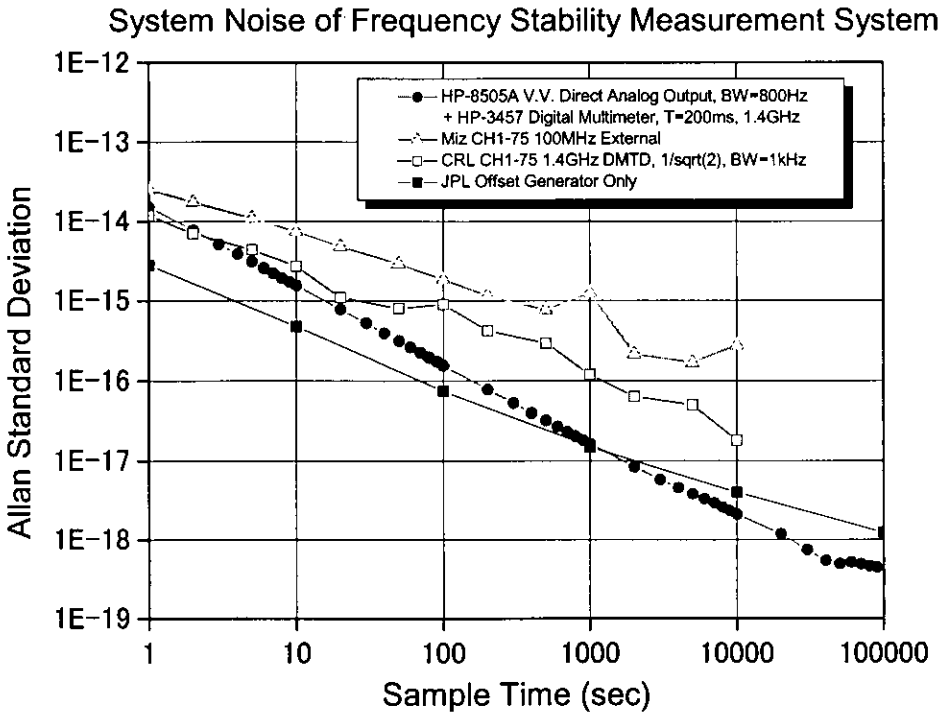

Figure 5-4 System noise of frequency stability measurement system.

The stability of the measurement system is better than 1.6×10^{-17} in ASD at 1000 second averaging time at 1.4GHz. This system noise level is obtained for the integration time of 200ms at each sampling when environmental temperature of the measurement system and PSOF cable are in stable condition.

Hamell et al. at JPL reported the best result of system noise as 1.5×10^{-17} at 100MHz in ASD for 1000 second averaging time using offset generator [22] as shown in Fig. 5-4. Though, it exceeds our results for the sample time more than 1000 second. The system noise level which is used for our laboratory measurement this time is better than that of any DMTD system as well as the offset generator system in long term.

5.2 Results of Laboratory Measurement

Change of power supply voltage influences most of instruments, and unexpected AC frequency signals mixed from power supply smears a reference frequency signal. Therefore, dependency of a phase variation characteristic to AC power supply voltage was investigated and SSB noise level of the distributed output signal was also measured. These measurements was carefully conducted using the developed ultra stable fiber optic signal distribution system while its environmental temperature was changing. The results are shown in this section.

5.2.1 Phase Variations Originated by AC Power Supply Voltage

A phase variation was monitored when AC power supply voltage of the system was changed from 85V to 115V by 15V step to test a dependency of the AC power supply voltage. Fig. 5-5 shows the results of this test. There is no relation between

the phase variation and the voltage change of the AC power supply.

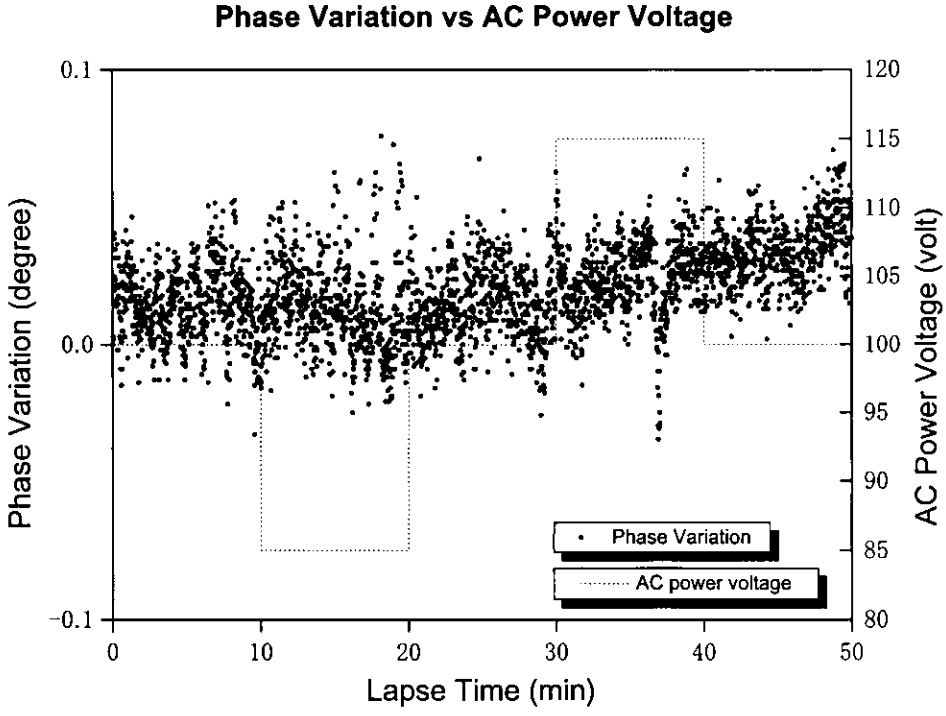

Figure 5-5 Phase variation characteristic originated by voltage change of AC power supply.

5.3.2 SSB Noise of Distributed Signal

SSB noise levels of the signals provided from the fiber optic frequency distribution system were measured by using Advantest corporation model TR-4133B spectrum analyzer.

The relations between a single-sideband spectral density $S_\nu(f)$, a spectral density $S_y(f)$ and Allan variance $\sigma_y^2(\tau)$ are explained in sections 2-1, 2-2 and 2-3. The equation is rewritten as

$$S_\nu(f) = \nu_0^2 \cdot S_y(f) = \nu_0^2 \cdot h_{-1} f^{-1} \tag{5-1}$$

where ν_0 is a frequency of distributing carrier signal and f denotes offset from the carrier signal. Substituting equation 5-1 into equation 2-11, $\sigma_y^2(\tau)$ is given as

$$\sigma_y^2(\tau) = 2 \cdot \ln(2) \cdot \frac{S_\nu(f)}{\nu_0^2 \cdot f^{-1}} \quad . \tag{5-2}$$

This equation converts single-sideband spectral density $S_\nu(f)$ to Allan variance $\sigma_y^2(\tau)$.

Fig. 5-6 shows the measured SSB noise spectrum of the output signal from Hewlett Packard model 8624B signal generator which has been used as a signal source in the laboratory measurements. Fig. 5-7 also shows the SSB noise spectrum of the distributed output signal of the antenna unit. The frequency span, resolution band width, and video band width of these SSB measurements are 20kHz, 100Hz and 10Hz. Fig. 5-8 shows wide sideband noise spectrum of the distributed output signal from the antenna unit with a frequency span of 100MHz, resolution band width of 10kHz, and video band width of 1kHz.

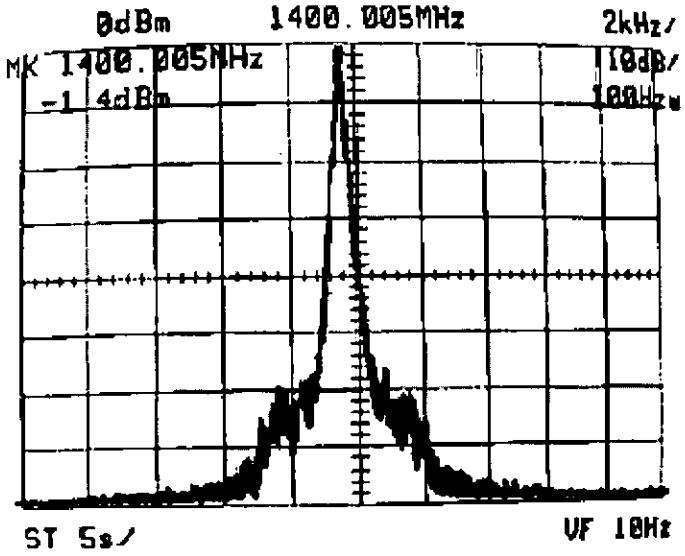

Figure 5-6 SSB noise spectrum of the output signal from Hewlett Packard model 8624B signal generator. The horizontal scale shows frequency in MHz with 2kHz per one division. The vertical scale shows a signal level in dBm with 10dB per one division and the maximum is 0dBm.

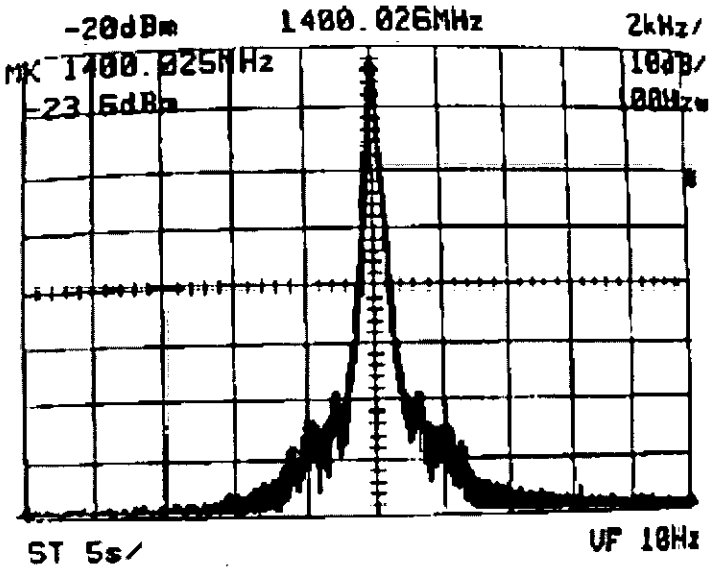

Figure 5-7 SSB noise spectrum of the distributed output signal from the antenna unit. The horizontal scale shows frequency in MHz with 2kHz per one division. The vertical scale shows a signal level in dBm with 10dB per one division and the maximum is -20dBm.

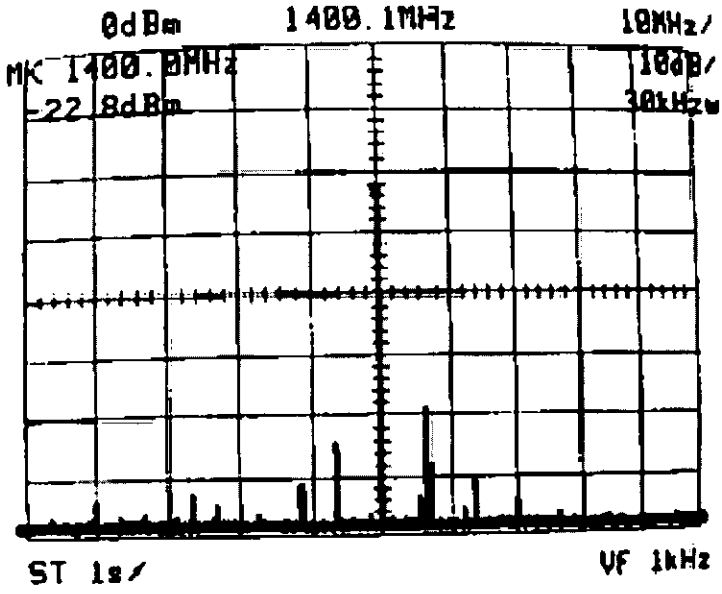

Figure 5-8 Sideband noise spectrum of the distributed output signal from the antenna unit. The horizontal scale shows frequency in MHz with 10MHz per one division. The vertical scale shows a signal level in dBm with 10dB per one division and the maximum is 0dBm.

The maximum SSB noise level of the output signal from the model 8624B signal generator at 1kHz offset is about 60 dB lower than the signal level in Fig. 5-6. This spectrum is measured with a resolution bandwidth of 100Hz and video band width of 10Hz by model TR-4133B spectrum analyzer. Because the maximum noise level in Fig. 5-6 is equal its power over the video band width of 10Hz, the carrier to noise ratio (C/N) per one hertz is -70dBc/Hz. This result is about 30 dB worse than that shown in the specification of the model 8624B signal generator. It is supposed that the spectrum analyzer increases SSB noise near the carrier signal source.

Substituting this value of -70 dBc/Hz to equation 5-2, $\sigma_y^2(\tau)$ is calculated as 7.0×10^{-23} when the integration time $\tau = 1$ second, the frequency of distributing carrier signal $\nu_0 = 1.4$GHz, and offset from the carrier $f = 1$kHz. The valiance 7.0×10^{-23} equals to 8.4×10^{-12} in ASD. This variation is limited by SSB characteristic near the carrier of the spectrum analyzer. HP-8624B itself has high C/N better than -100 dBc at 1kHz offset from its specification. The value -100 dBc in SSB noise relates to 2.7×10^{-13} in ASD. Comparing the measured and specification values of HP-8624B, the HP-8624B used for laboratory measurement is not stable enough in ASD. A relative phase variation between the reference signal and the signal which is distributed through the tested system are measured in the laboratory measurement. Thus, this phase stability of the signal source does not affect the laboratory measurements even if the test signal source is unstable a little.

Fig. 5-8 shows a lot of high sideband noises beside the carrier frequency signal. These sideband noise will be rejected when additional extra phase lock oscillator is installed into the output line of the antenna unit. This extra phase lock oscillator will also increase the carrier to noise ratio of the output signal from the antenna unit.

5.2.3 Phase Variations According to Environmental Temperature Change

The phase variations of the distributed signals from the control unit to the antenna unit were measured, to show the stability performance of the developed ultra phase stable frequency distribution system. The temperatures of the test chamber, in which PSOF cable was placed, were varying with the range of 10°C at the rates of 10°C/15minutes and 10°C/12hours. The former temperature variation rate is equal to one observation time span in differential VLBI. The latter temperature variation rate is similar to the daily environmental temperature variation.

The results of the measurement is shown in Fig. 5-9. The actual phase variations of transmitted reference frequency at the antenna unit are shown for the periodic change of the temperature of 10°C at the rate of 10°C/15minutes. The lines with circles and without circles represent that of the closed phase-lock loop is disabled (control-off) and enabled (control-on) respectively. The phase variations are larger than 0.4 degrees in peak-to-peak in the former case. In the latter case, the phase variation is less than 0.1 degrees in peak-to-peak, which is limited both by the remained phase variations in the cable and internal random noises.

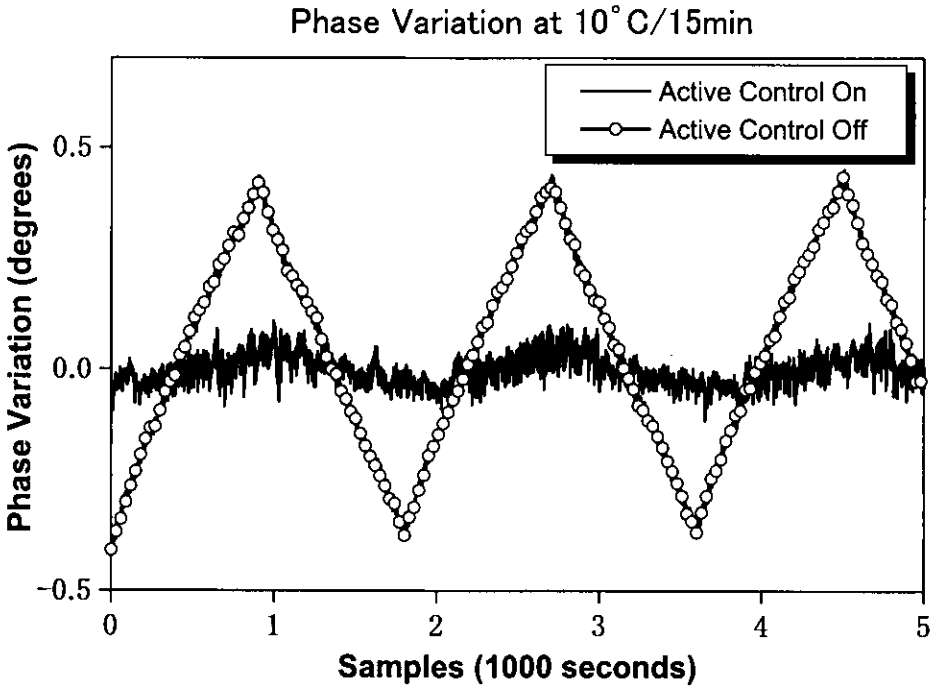

Figure 5-9 Actual phase variation caused by the PSOF cable delay change in the temperature variation at the range of 10°C and the rate of 10°C/15minutes.

The phase stabilities of the developed ultra stable frequency distribution system in ASD are shown in Fig's 5-10 and 5-11, for the temperature variation of 10°C at the rates of 10°C/15minutes and 10°C/12hours, respectively.

From the Fig. 5-10, the phase stability in ASD is about 1.2×10^{-15} for control-off and 1.3×10^{-16} for control-on at 1000 second in averaging time for the temperature variation at the rate of 10°C/15minutes. The phase stability for control-on, which is 1.3×10^{-16} in ASD, is 1.3 times worse than the required stability at 1000 second in the averaging time. Below 100 second in the averaging time, the phase stability for control-on is worse than that of control-off. From the Fig. 5-11, the phase stability in ASD is about 3.8×10^{-17} for control-off and 7.5×10^{-17} for control-on at 1000 second in averaging time for the temperature variation at the rate of 10°C/12hours. Again, below 4300 second in averaging time, the phase stability for control-on is worse than that of control-off. However, in this case the measured ASD always kept below the required stability. In Fig. 5-11, the stabilities in ASD are about 1.7×10^{-17} and 1.1×10^{-17} at 10,000 second in averaging time for control-off and control-on respectively in a temperature variation rate of PSOF cable at 10°C/12hours.

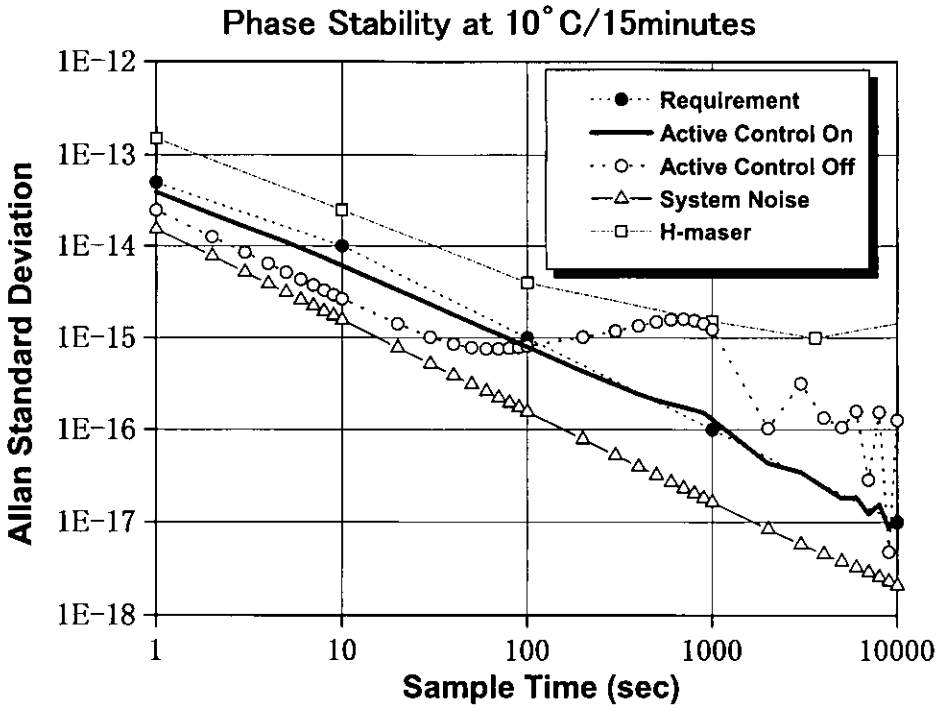

Figure 5-10 Stabilities in ASD when the temperature of PSOF cable varies by 10°C at the rate of 10°C/15minutes.

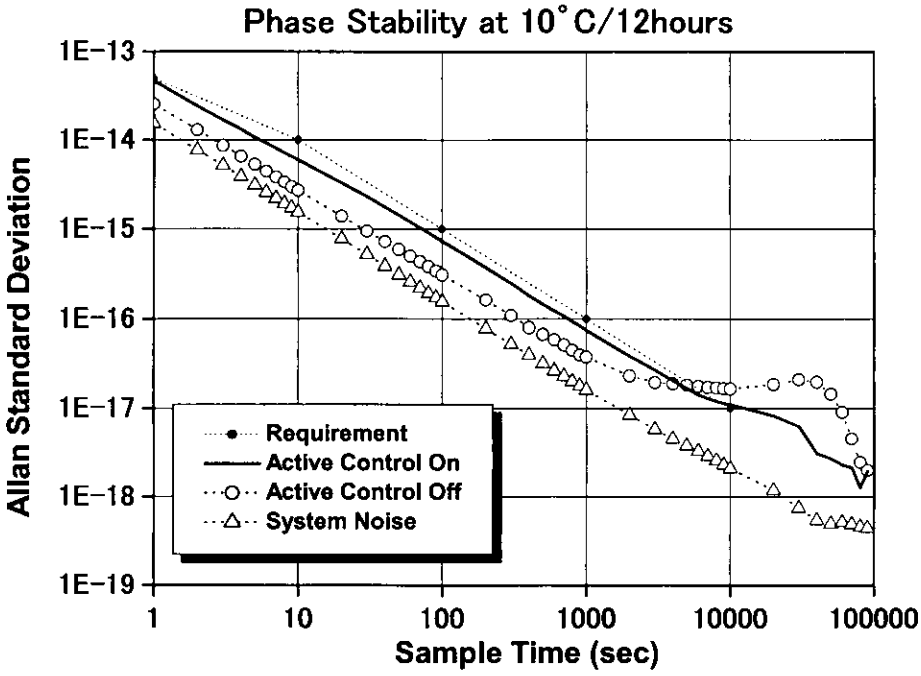

Figure 5-11 Stabilities in temperature variation of PSOF cable at the range of 10°C and the rate of 10°C/12hours.

In Fig. 5-12, filled circles show a response of the developed frequency distribution system to a step-like phase change for control-on. The phase variation is monitored after the depressed ring of PSOF cable with 20cm diameter has been rapidly released. Open circles show a response of this system to a step-like phase change for control-off.

The step-like phase change was given about 0.15 degrees as shown in Fig. 5-12. The figure shows the phase compensator responds to the step-like phase change within 1 second and it takes about 6 seconds to compensate this step-like phase disturbance. Because the time constant of a loop in the phase compensator is designed to be near 1 second, the response time of 1 second coincides with the designed time constant.

On the other hand, the phase compensation would be too slow in consideration of the response time of 0.1 second for the ODM. There are some possible reasons for such slow phase compensation. One is the AC bias which is added to the DC drive voltage for the ODM in order to actuate the ODM against a backlash. The other one is the unsuitable DC drive voltage or noise of the voltage.

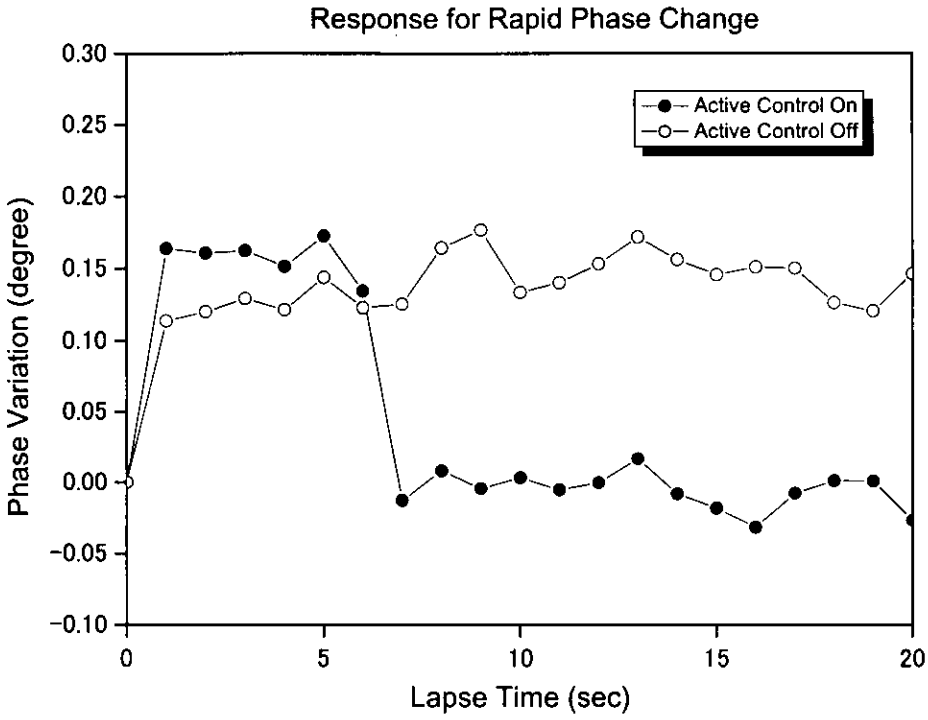

Figure 5-12 Response of the system to a step-like phase change.

CHAPTER 6

DISCUSSIONS AND CONCLUSIONS

6.1 Discussions

The performance of the phase compensator, demonstrated in Fig. 5-9, shows that the phase variation is less than 0.1 degrees in peak-to-peak when the system is in control-on and the temperature change at the rate of 10°C/15minutes. This variation consists of both by the phase variations in the cable and internal random noises. The short term phase fluctuations of internal random noise in the Fig. 5-9 could be estimated as 0.05 degrees. After the phase variation of internal random noise is excluded, the phase variation induced in the cable is estimated as 0.05 degrees in peak-to-peak. It is clear that the developed ultra stable fiber optic frequency distribution system reduces the actual phase variations of 0.4 degrees in peak-to-peak to one tenth of its phase variation when the system is in control-on.

The measured phase variation of the developed ultra stable fiber optic frequency distribution system are below the required stability except for the case when the averaging time is 1000 second and the temperature variation rate of the PSOF cable is 10°C/15minutes. The temperature variations at the rate of 10°C/15minutes or 10°C/12hours, which are inflicted on the PSOF cable in this

measurement, are about 10 times severer than that in the environment where a PSOF cable is utilized as an actual VLBI system. So that, the stability at 1000 second in the averaging time is expected to be better than the required stability when this distribution system is actually installed.

The phase stability in control-on is worse than that in control-off in the range of the averaging time less than 100 second and 4300 second for a temperature variation rate at 10°C/15minutes and 10°C/12hours respectively. This degradation of the stability is caused by the response with different hysteresis in backward and forward movement of an ODM. For this reason, an ODM that has no such different hysteresis is required for the further improvement of the phase stability in control-on.

The developed ultra stable fiber optic frequency distribution system compensates the step-like phase change of 0.15 degrees within 6 seconds. Considering bending and twisting of a PSOF cable, fortunately such rapid step-like phase change will not be generated under the condition while the antenna is continuously tracking a star in a conventional VLBI observation. However, if this system is applied to the instrument which requires rapid phase compensation such as an optical interferometer, the improvement of the response time is expected by replacing the present ODM to no backlash model which will not require the additional digital servo loop circuit to drive it.

To apply this developed ultra stable fiber optic frequency distribution system for a reference frequency of a down converter in a VLBI observation system, the purity of the output signal should be considered. The phase stability of the 1.4GHz output signal from the antenna unit is smeared by power supply frequency while the signal is processed in the unit. A phase stability of the signal, which is modulated by a discrete noise such as a power supply frequency, is investigated by Yoshimura

et al. [18] and discussed in section 2.4. When a discrete noise is assumed as a modulating frequency, the two-sample standard deviation of a phase variation is expressed by the equation 6-1 which is similar to the equation 2-39

$$\sigma_y(\tau) = \varphi_m \times \left(\frac{f_m}{\nu_0}\right) \times \frac{\sin^2 u}{u} \quad , \tag{6-1}$$

where φ_m denotes a modulation index which is considered as $(N/C)^{1/2}$, u equals to $\pi f_m \tau$ and f_m denotes a modulating frequency. The RMS phase variation $\langle \Delta\varphi^2 \rangle^{1/2}$ is expressed as the equation 4-1. Substituting the σ_y, which is estimated as the allowed value from the equation 4-1, to the equation 6-1, φ_m is given when sin u is assumed as maximum. The calculated CNR of the system is about 65.6dB when the modulating frequency is assumed as 50Hz. The measured CNR in Fig. 5-7 is about 60dB at 1kHz offset with 10Hz video bandwidth. This value equals to 70dB at 1Hz bandwidth. This measured CNR is comparable with the calculated CNR. This means that the sideband spectrum in the Fig. 5-7 is generated by power supply frequency. However, the measured CNR value of 70dB is obtained through a video filter with the narrow bandwidth of 10Hz. Therefore, actual CNR of the output signal from the antenna unit without a narrow filter is worse than that of the measured CNR with narrow video filter. This means actual CNR in the output signal from the antenna unit would be less than 70dB. The RIN of the laser diode used in the system has the CNR of -115dB/Hz [28]. The CNR of the PIN photo diode is better than -100dB/Hz according to the estimation in section 4.3.3.2 and the estimation by Nishio [21]. The degradation of CNR to 70dB/Hz will be caused in electronic components other than laser diode and PIN photo diode. To achieve better CNR of 1.4GHz output signal from the antenna unit, a phase-locked oscillator with good signal purity is required for the further improvement.

The maximum transmission distance of the frequency distribution depends on

the CNR of the loop in the frequency distribution system. The relation between the ASD of the frequency distribution system and the CNR is expressed in equation 4-1. Substituting the allowed value 5×10^{-14} of stability that is estimated in section 4.1.2 to the equation 4-1, the CNR is calculated as 68.9dB. The margin is 1.1dB against the measured CNR of the system. The maximum transmission distance through an optical fiber cable is then estimated as 2.75km since the transmission loss of the PSOF cable is about 0.4dB/km. This maximum transmission distance is extended when the phase-locked oscillator with good signal purity is replaced with the one used now, and when the output power of the laser diode is increased, because of increasing CNR margins. A relation between the output power to an optical fiber from a laser diode and an output power of a modulated carrier is expressed as equation 4-15.

A noise from of a laser diode deteriorates SNR of an output carrier signal to an optical fiber. Therefore the stability of the system decreases according to the equation 4-1. The noises from a laser diode are classified as quantum shot noise and mode hopping noise that is generated while the laser diode is in longitudinal mode [35]. The mode hopping noise is generated against the variations of drive current and environmental temperature. These quantum shot noise and mode hopping noise are suppressed under the cooled condition and stable environmental temperature and do not affect in digital optical communications. Though, returned optical signals from an optical fiber to a laser diode and modal noise cause disturbance in SNR. To avoid the influence of a returned optical signal into a laser diode, it is recommended to use an optical isolator and to use distributed feedback (DFB) or distributed bragg reflector (DBR) laser diode [3][35]. Further more, the modal noise is not generated in a single mode fiber. In the developed ultra stable fiber optic frequency distribution system, so that a DFB laser diode with single mode operation is used.

Some new photonics reference frequency distribution systems, in that the difference of frequency of two different wavelength lasers was used as a distributing frequency, demonstrated a capability [33][34]. If the distributing frequency is assumed to be 100GHz and two wavelengths of lasers also assumed to be 1.55μm and 1.5492μm, the difference of a refractive index of two wavelengths in fiber medium causes delay difference of ±3.2ps per one kilometer, because the delay difference in fiber medium of PSOF cable is estimated as ±4ps/nm/km for 1.55μm wavelength band. The value of this ±3.2ps equals to ±115.2 degrees at 100GHz. There is no delay difference in 1.3μm wavelength band because of no difference of a refractive index in fiber medium for this wavelength band. These delay differences are mostly caused while an optical fiber layed in an environment where the temperature shows daily variation. The thermal coefficient of PSOF cable is about the order of 5ps/km/°C. The phase variation of 0.864×10^{-3} degrees at 100GHz per one kilometer is generated by the difference of the refractive index of PSOF cable for the 1.55μm and the 1.5492μm wavelengths when the environmental temperature changes 5 °C. Thus, even for the photonics reference frequency distribution systems, these phase variations should be compensated. The phase compensation method that uses ODM in the developed actively stabilized fiber optic frequency distribution system could contribute for the phase stabilization of these photonics reference frequency distribution systems. Therefore, the fiber optic systems are widely used in the signal transmission field lately. The ODM is suitable to compensate the phase variation in these fiber optic signal transfer systems.

6.2 Conclusions

The ultra stable fiber optic frequency distribution system has been developed

and its performance is demonstrated. It is the first ODM application to be implemented for use in fiber optic frequency distribution system. It is the first direct DC analog output usage of a vector voltmeter to be implemented for use in a frequency stability measurement system. The system noise level of this measurement system in the laboratory is better than any dual mixer time difference systems. The stabilities in ASD are about 7.5×10^{-17} and 1.1×10^{-17} at 1000 second and 10,000 second in averaging time respectively, in temperature variations of PSOF cable at the range of 10°C and the rate of 10°C/12hours. This system has the best stability in frequency distribution systems developed so far.

This system can be applied for the distribution of reference frequency from the ultra stable new frequency standard such as an ion storage frequency standard, to the differential VLBI system used for the precise measurements of the distance to galactic radio sources and to the connected radio interferometer in sub-millimeter range.

APPENDIX A

Calculation Program of Allan Standard Deviation

```
'*************************************************************************
'*                                                                       *
'*                                                                       *
'*        ALLAN VARIANCE EVALUATION SYSTEM FOR VECTOR VOLT METER         *
'*                   --- ALLAN VARIANCE CALCULATION ---                  *
'*                                V 1.0                                  *
'*                        June 20, 1998 K.-H. SATO                       *
'*                                                                       *
'*                                                                       *
'*************************************************************************
'
'This program calculates ALLAN VARIANCE using the data obtained at every
'1 second by a vector voltmeter phase measurement at 1400MHz.
'
'      HP-8508 Vector Voltmeter and HP-3457A multimeter version
'
'      Summation limit is N+1-2n. N is defined as data number ID-1.
'
```

```
        DMN = 300000 : 'Dimension Number
        dim DD#(DMN)
        BLK50$ = "                                                    "
'
*BEGIN
'
        color 0,15 : cls : locate 3,1
'
        print "*******************< Allan Variance >*******************"
        beep : locate 3,2
        input "Data File Name C:\WORK\########.DAT";DFN$
        open "C:\WORK\"+DFN$+".DAT" for input as #1
        open "C:\WORK\"+DFN$+".ALN" for output as #2
'
        SPLINT% = 1
'
*KYI0   locate 3,3
'
        beep : input "Sampled Data Number (max 300,000)";CONTMAX!
        if CONTMAX! > DMN then locate 3,3 : print BLK50$ : goto *KYI0
'
        ID = 0
        DSUM# = 0#
        IRC = 0
'
        for IR = 1 to int(CONTMAX!)
'
'1.984126984D-12 : conversion factor for degree to time interval
'1 / 1400E+6 / 360 : time interval for 1 deg in 1400MHz (sec)
```

```
'Phase difference = Multi meter readings * 100.0
'
          input #1, NN,DD$  : AAA# = val(DD$) * 1.984126984D-10
          if abs( AAA# ) < .000000000715# then goto *GDAT
          locate 20,13 : color 2
          print "Rejected   ";AAA#,IR
          color 0 : IRC = IRC + 1 : goto *NXTI
'
*GDAT     locate 70,22 : print IR
'
          ID = ID + 1
          DD#(ID) = AAA#
'
          if eof(1) then *REND
'
*NXTI  next IR
'
*REND  IDCNUM = ID
'
'
       for IPOW = 0 to 4
       for IFLX = 1 to 9
'
          SKIP = int( IFLX*(10^IPOW) + .5 )
          CALINT = SKIP
'         if CALINT > 10000 then goto *CEND
          CALEND = 10 ^ int( log( IDCNUM ) / log( 10! ) )
          if CALINT > CALEND + 1 then goto *CEND
'
```

```
          FDFSUM# = 0#
'         tau = NN*tau0, tau0:interval, NN:1,2,3,.....,N/2
          NN = SKIP
'         total sampled number as N+1 = IDCNUM
          SUMN = IDCNUM - 2*NN
'
          for I = 1 to SUMN
             I1 = I + 2*NN
             I2 = I + NN
             I3 = I
             DDI1# = DD#(I1)
             DDI2# = DD#(I2)
             DDI3# = DD#(I3)
             FDFSUM# = FDFSUM# + ( DDI1# - 2#*DDI2# + DDI3# )^2
          next I
'
*SEND     SIGM# = sqr( FDFSUM#/( 2# * cdbl(SUMN) * cdbl(NN)^2 ) )
'
          locate 15,11 : print BLK50$
          locate 15,11 : print "Allan SD (";CALINT;" sec) is  "
          locate 40,11 : print SIGM#
'
          print #2,CALINT;SIGM#
'
       next IFLX
       next IPOW
'
*CEND  close #1 : close #2 : end
```

APPENDIX B

Specification of HP-8508A Vector Voltmeter

Frequency Range	300kHz - 2GHz
Maximum Input	16dBm, ±50Vdc
Measurement Range	
A and B Channel Maximum	Magnitude measurements
	3dBm, 300kHz-1MHz, 1GHz-2GHz
	13dBm, 1MHz-1GHz
	Phase measurements
	3dBm, 300kHz-2GHz
A (Ref) Channel minimum	-47dBm, 300kHz-3MHz
	-57dBm, 3MHz-2GHz
B (Meas) Ch. noise floor	-87dBm, 300kHz-2GHz
Measurement Bandwidth	1kHz (nominal)
Input Crosstalk	>100dB, 300kHz-500MHz
	>80dB, 500MHz-1GHz

	>70dB, 1GHz-2GHz
Impedance	SWR<1.2, 300kHz-1.5GHz
	SWR<1.5, 1.5GHz-2GHz

Magnitude Characteristics

Resolution:	3 ½ digits

Phase Characteristics

Display Range:	-179.9 to +180.0 degrees
Display Resolution:	0.1 degrees

Search and Lock Time

Automatic tuning starts from lowest frequency and searches consecutive bands. Total search and lock time depends on the number of bands to be scanned and the lockup time within the selected band.

Process Start Time:	50ms after lock is lost.
Lockup (within 1 range):	40ms, frequencies up to 3MHz
	20ms, frequencies greater than 3MHz
Ranges (MHz):	0.1-0.2, 0.2-0.6, 0.6-1, 1-3, 3-5, 5-8, 8-15, 15-25, 25-50, 50-80, 80-150, 150-250, 250-500, 500-1000, 1000-2000

Rear Panel Outputs:

Normal Operation: Provides an analog representation of the digital display values, including internal instrument correction factors.

OUTPUT 1 corresponds to DISPLAY 1, OUTPUT 2 corresponds to DISPLAY 2.

Range: 0 to ±1999 display counts.

Sensitivity: 1mV represents 1 display count (nominal).

For readings greater than ±1999 counts, the rear panel output voltage will remain fixed at ±2.0 Volts.

Display resolution can be controlled by manual ranging.

Update rate: Approximately 3 readings per second.

Direct Analog Output: Provides continuous direct output from the internal magnitude and phase detectors through 800Hz low-pass filters. No internal correction is applied.

OUTPUT 1 corresponds to linear magnitude (A or B selected by front panel control).

Sensitivity: 1V equals displayed full scale deflection (nominal). Can be controlled by manual ranging.

OUTPUT 2 corresponds to B-A phase.

Sensitivity: 10mV per degree (nominal).

Phase Jitter: <3 deg rms (typical, A=100mV, B=100μV)

ACKNOWLEDGMENTS

I would very much like to thank all the people who provided so much assistance, guidance, and support for developing the system and completing this work.

First, I feel greatly indebted to my advisor, Dr. Nobuyuki Kawano, who encouraged me to complete the work in this Thesis. I am also grateful to Dr. Tadayoshi Hara and Dr. Masanori Nishio, for their patience, understanding, and helpful advice. Special thanks are owed to Mr. Seisuke Kuji and Mr. Kazuyoshi Asari for the technical assistance they gave so consistently and enthusiastically. I wish to express my hearty gratitude to Mr. A. Maruyama and Mr. T. Tsukamoto of Anritsu Corporation for the integration of the system.

I am also express my sincere appreciation to the staffs at Mizusawa Astrogeodynamics Observatory, National Astronomical Observatory for their kind help.

LIST OF REFERENCES

[1] G. F. Lutes, "Development of Optical Fiber Frequency and Time Distribution System," in *Proc. of the 12th Annual Precise Time and Time Interval (PTTI) Applications and Planning Meeting*, pp. 243-261, 1980.

[2] G. F. Lutes and A. Kirk, "Reference Frequency Transmission Over Optical Fiber," in *Proc. of the 18th Annual Precise Time and Time Interval (PTTI) Applications and Planning Meeting*, pp. 385-394, 1986.

[3] G. F. Lutes,"High Stability Frequency and Timing Distribution Using Semiconductor Lasers and Fiber Optic Links," in *Proc. of the SPIE,* vol. 1043, pp. 263-271, 1989.

[4] D. K. Davies and A. P. Goutzoulis, "Wavelength-multiplexed analog fiber optic link for wideband radio-frequency and local oscillator signal transmission," *Optical Engineering,* vol. 31, 11, pp. 2323-2329, 1992.

[5] T. Y. Otoshi, M. M. Franco and G. F. Lutes, "Performance of a 12-Ghz Fiber-Optic System for Beam-Waveguide Antenna Stability Testing," TDA progress report, PR 42-109, pp. 105-113, May 1992.

[6] M. Calhoun and P. Kuhnle, "Ultrastable reference Frequency Distribution Utilizing a Fiber optic Link," in *Proc. of the 24th Annual Precise Time and Time Interval (PTTI) Applications and Planning Meeting*, pp. 357-364,

1993.

[7] R. Dragonette and J. J. Suter, "Performance of Low-Cost Commercisl Fiber-Optic Tranceivers for Reference Frequency Distribution," in *Proc. of the 24th Annual Precise Time and Time Interval (PTTI) Applications and Planning Meeting*, pp. 343-356, 1993.

[8] O. I. Kotov, L. B. Liokumovich and V. M. Nicolaev, "Phase-Stable Fiber Optic Systems for Reference RF Signals," in *Proc. of the SPIE,* vol. 2321, pp. 489-492, 1994.

[9] R.L. Tjoelker, C. Bricker, W. Diener, R.L. Hammel, A. Kirk, P. Kuhnle, L. Maleki, J.D. Prestage, D. Santiago, D. Seidel, D.A. Stowers, RL. Sydnor and T. Tucker, "A Mercury Ion Frequency Standard Engineering Prototype for the NASA Deep Space Network," in *Proc. 50th Ann. Symp. Freq. Control,* pp.1073-1081, June, 1996.

[10] T. Sasao, "VERA (VLBI Exploration of Radio Astrometry)," in *Proc. of the Technical Workshop for APT and APSG 1996*, pp. 70-74, 1997.

[11] T. Kakuta and S. Tanaka, "LCP coated optical fiber with zero thermal coefficient of transmission delay time," in *Proc. 36th International Wire and Cable Symposium*, pp. 234-240, 1987.

[12] K.-H. Sato, T. Hara, M. Fujishita, S. Kuji, S. Tsuruta, Y. Tamura, T. Sasao, K. Sato and S. Manabe, "Application of phase-stabilized optical fiber in transmission of reference and IF signals in VLBI observation," *IEEE Trans. On Instrumentation and Measurement*, vol. IM-41, no.3, pp.385-389, 1992.

[13] G. F. Lutes and L. E. Primas, "State-of-the-art fiber optics for short distance frequency reference distribution," TDA progress report, PR 42-97, pp. 81-87, May 1989.

[14] L. E. Primas, G. F. Lutes and R. L. Sydnor, "Stabilized fiber-optic frequency

distribution system," TDA progress report, PR 42-97, pp. 88-97, May 1989.

[15] D. Johnson, M. Calhoun, R. Sydnor and G. Lutes, "A wide-band fiber optic frequency distribution system employing thermally controlled phase compensation," in *Proc. of the 24th Annual Precise Time and Time Interval (PTTI) Applications and Planning Meeting*, pp. 365-374, 1993.

[16] F. L. Walls and D. W. Allan, " Measurements of Frequency Stability," in *Proc. Of the IEEE*, vol. 74, pp. 162-168, Jan. 1986.

[17] A. R. Thompson, J. M. Moran and G. W. Swenson, Jr, "Interferometry and Synthesis in Radio Astronomy," A Wiley-Interscience Publication, 1986.

[18] K. Yoshimura and M. Kobayashi,"Frequency Stability due to Discrete Noise in Frequency Synthesizers," *The Transactions of the Institute of Electronics and Communication Engineers of Japan. C* , vol. 54-C, 6, pp. 507-513, 1971.

[19] C. A. Greenhall, "Frequency Stability Review," TDA progress report, PR 42-88, pp. 200-212, February, 1987.

[20] R. T. Logan, G. F. Lutes, L. E. Primas and L. Maleki, "Design of a Fiber-Optic Transmitter for Microwave Analog Transmission with High Phase Stability," TDA progress report, PR03-32, pp. 27-33, 1990.

[21] M. Nishio, S. Kawashima, C. Torii, H. Nakajima, T. Takabayashi, K. Nishikawa, N. Futagawa and S. Tanaka, "An Optical Fiber Phase Lock Network of a Radio Interferometer," in *Proc ICALEPCS '91,* 1991.

[22] R. Hamell, P. Kuhnle and R. Sydnor, "An improved offset generator developed for Allan deviation measurement of ultra stable frequency standards," in *Proc. of the 23rd Annual Precise Time and Time Interval (PTTI) Applications and Planning Meeting,* pp. 209-218, 1992.

[23] M. Calhoun and P. Kuhnle and J. Law, "Fiber optic reference frequency

distribution to remote beam waveguide," in *Proc. of the 26th Annual Precise Time and Time Interval (PTTI) Applications and Planning Meeting,* pp. 415-426, 1995.

[24] H. F. Taylor, "Bending effects in optical fibers," *J. Lightwave Technology,* vol. LT-2, pp.617-628, Oct. 1984.

[25] J. Saijonmaa and D. Yevick, "Beam-propagation analysis of loss in bent optical waveguides," *J. Opt. Soc. Am.,* pp. 1785-1791, 1983.

[26] "RF/Microwave Fiber Optic Link Design Guide," ORTEL corporation, May, 1990.

[27] "Laser Diode Module Model NDL7610PA Data Sheet," NEC corporation, 1994.

[28] "Laser Diode Module Model NDL7710PA Data Sheet," NEC corporation, 1994.

[29] "Photo Diode Module Model NDL5422P Data Sheet," NEC corporation, 1994.

[30] "Optical Delay Line Module ODL-610 Data Sheet," Santec corporation.

[31] "Double Balanced Mixer Model R&K M-14LL Data Sheet," R&K corporation.

[32] E. I. Ackerman, "System-Level Performance Evaluation of Microwave Fiber-Optic Links," Thesis (Ph. D.) Drexel University, 1994.

[33] W. Shieh, S.X. Yao, G. Lutes and L. Maleki, "Microwave Signal Mixing by Using a Fiber-Based Optelectronic Oscillator for Wavelength Division Multiplexed (WDM) Systems," JPL Technical Report, Dallas, Texas, USA, Feburuary 18-21, 1997.

[34] E. Brown, S. Verghese, K.A. McIntosh, "Terahertz photomixing in low-temperature-grown GaAs," Proc. SPIE, Vol. 3357, pp. 132-142, 1998.

[35] H. Yonezu, "Optical Communication Devices (light emitting devices and photo acceptance devices)," Kougaku tosho publishing company, ISBN 3054-20194-2213, 1986 (in Japanese).

[36] K.-H. Sato, T. Hara, S. Kuji, K. Asari, M. Nishio and N. Kawano, "Development of an Ultra Stable Fiber Optic Frequency Distribution System using an Optical Delay Control Module," *IEEE Trans. On Instrumentation and Measurement*, vol. IM-49, no.1, pp.19-24, 2000.